CHARACTERIZATION OF MULTI-BIT DIFFERENTIAL CHANNELS: A MODIFIED MODAL SCATTERING PARAMETER APPROACH

by

Joel Ryan Martin

B.S in Engineering Physics, University of Pittsburgh, 2003

Submitted to the Graduate Faculty of

the School of Engineering in partial fulfillment

of the requirements for the degree of

Master of Science in Electrical Engineering

University of Pittsburgh

2006

UNIVERSITY OF PITTSBURGH

SCHOOL OF ENGINEERING

This thesis was presented

by

Joel Ryan Martin

It was defended on

July 20, 2006

and approved by

Donald M. Chiarulli, Professor, Department of Computer Science

Steven P. Levitan, Professor, Department of Electrical and Computer Engineering

William Stanchina, Chairman and Professor, Department of Electrical and Computer Engineering

Joel Falk, Professor, Department of Electrical and Computer Engineering

Thesis Advisors: Donald M. Chiarulli, Professor, Department of Computer Science,

Steven P. Levitan, Professor, Department of Electrical and Computer Engineering

ABSTRACT

CHARACTERIZATION OF MULTI-BIT DIFFERENTIAL CHANNELS: A MODIFIED MODAL SCATTERING PARAMETER APPROACH

Joel Ryan Martin, M.S.

University of Pittsburgh, 2006

High speed inter-chip interconnects have reached and exceeded the multi-gigabit per second benchmark using differential signaling. Multi-bit differential signaling (MBDS) has been proposed as a solution to the $2n$ per n bit pin requirement of classical differential channels. MBDS does not currently have a modal characterization similar to the common and differential mode analysis developed for differential signaling that would allow a description of MBDS channel behavior. This thesis introduces a modal characterization of MBDS links via the development of modal scattering parameters that allow the analysis of the communications channel. Simulation results are presented in conjunction with data collected from a fabricated printed circuit board designed for MBDS links. Multiple printed circuit board layouts are be presented for analysis and design comparison. It is shown that the performance of MBDS links can be severely impacted by unoptimized PCB layout.

TABLE OF CONTENTS

LIST OF TABLES

LIST OF FIGURES

1.0 INTRODUCTION

Many current problems in computer system design are centered around the inability to achieve arbitrarily high bandwidth between several discrete integrated circuits. Printed circuit board (PCB) traces are a major barrier to gigabit-per-second, low power interconnects due to the domination of transmission line effects at high frequencies. The length of PCB traces becomes comparable to the wavelength of the propagating signal at a few hundreds of megahertz and the resulting wave behavior of both the current and voltage dominate.

A common solution for high speed short range links is differential signaling. Differential techniques are used in many current backplane and memory interconnect technologies such as Advanced Micro Devices' Hypertransport bus specification [10]. Differential signaling has been the focus of much research and is a mature technology with the supported development of design techniques at all levels of operation from the driver and receiver circuitry to methods that allow for the optimization of the PCB design.

Multi-Bit Differential Signaling (MBDS) has been proposed as an extension to differential signaling that seeks to improve upon the area, power and fanout requirements of differential links [5]. MBDS retains all the advantages of differential signaling with the ability to scale the capacity of the link as needed to meet the demands of the interconnect.

Scattering parameters (S-parameters) have been used by the RF community as a convent way to characterize a channel, circuit or system and are based on a per port view of the system. Differential systems are not well described by a 'per-port' view of the word; it is the behavior of each port relative to others in the system that best characterizes the link. A mode specific formulation of S-parameters has been developed that allows for the quantification of the channel in a domain that naturally meshes with the description of differential circuits [2].

Differential mode specific analysis of a channel via multi-modal S-parameters can be performed and the channel performance understood and refined. MBDS does not have an equivalent mode-specific formulation. *A priori* analysis of the channel can only be performed via traditional linear network operators such as S-parameters. Fundamental signal integrity issues in the end-to-end design of an MBDS link can not be adequately answered without trial an error, either by simulations or actual fabrication of MBDS links.

This thesis presents a method to characterize MBDS channels. The technique presented allows for the description of any MBDS link configuration and is used to characterize several proposed PCB designs for two MBDS configurations. Simulations of several PCB topologies as well as collected test data are presented. This chapter will introduce several motivating technologies and techniques that will be used to develop the characterization and concludes with a problem statement. Chapter 2 outlines prior work on the analysis of differential links of which this thesis will build on. Chapter 3 reviews the development of multi-modal scattering parameters for MBDS channels. Simulation results and collected test data are presented in Chapters 4 and 5 with concluding remarks in Chapter 6.

1.1 MOTIVATION

1.1.1 Transmission Line Effects

The relationship between voltage and current of *n* coupled transmission lines with the major dimension oriented along the z-axis are derived from Maxwell's equations and are collectively known as the the telegraphers equations [13]. A conductor of length l begins to exhibit transmission line behavior when any physical dimension of the line approaches and exceeds the wavelength of the signal traveling along the line. The equations that describe the resulting voltage and current wave through a transmission line in the frequency domain are defined as,

$$-\frac{\partial}{\partial z}\vec{\mathbf{V}}\left(z,t\right)=\mathbf{Z}\vec{\mathbf{I}}\left(z,t\right)e^{j\omega t}, \tag{1.1}$$

and

$$-\frac{\partial}{\partial z}\vec{\mathbf{I}}\left(z,t\right)=\mathbf{Y}\vec{\mathbf{V}}\left(z,t\right)e^{j\omega t}, \tag{1.2}$$

where the $n \times n$ matrices $\mathbf{Z}$ and $\mathbf{Y}$ are the frequency dependent impedance and admittance matrices, respectively.

The $n \times 1$ vectors $\vec{\mathbf{V}}$ and $\vec{\mathbf{I}}$ represent the state of the transmission line as a function of time and position with the elements of the vectors describing line i. Both $\mathbf{L}$ and $\mathbf{C}$ are determined by the geometric structure of the transmission line, the conductor and dielectric properties and the frequency of the propagating signal.

Taking the derivative of Equation 1.2 in the frequency domain and substituting the result into Equation 1.1 gives,

$$-\frac{d^2}{dz^2}\vec{\mathbf{V}}\left(z,t\right) = \mathbf{ZY}\vec{\mathbf{V}}\left(z\right)e^{j\omega t}, \tag{1.3}$$

while the equivalent transform for the current yields,

$$-\frac{d^2}{dz^2}\vec{\mathbf{I}}\left(z,t\right) = \mathbf{YZ}\vec{\mathbf{I}}\left(z\right)e^{j\omega t}. \tag{1.4}$$

The solutions to these equations are of the form of decaying exponential forward and backward traveling waves that propagate though the structure on each conductor. The matrix product $\mathbf{LC}$ contains all physical information about the structure and will change as any physical property such as conductor width varies. These changes directly impact the characteristic impedance, $\vec{\mathbf{Z}}_O$ defined as the ratio of the voltage wave to the current wave. Proper impedance matching a the ends of a transmission line is a critical factor in transmission line behavior as mismatches at either end of the line create boundary conditions that allow backward traveling wave solutions to 1.3 and 1.4 to be non-zero.

Ports are defined as an end of the transmission line where $z = 0$ or $z = l$ where l is the length of the transmission line. An n conductor transmission line will have $2n$ ports for each line end. This thesis will define ports 1 through n to be the plane where $z = 0$ and ports $n + 1$ through $2n$ as the plane where $z = l$.

Transmission line effects present an upper bound on the capacity of electrical channels. Miller and Ozaktas have shown that the maximum bit rate capacity of a transmission line that is dominated by inductive and capacitive effects is,

$$B \cong 10^{15}\frac{A}{l^2}, \tag{1.5}$$

where A is the cross-sectional area of the conductors, l is the length of the line and $\frac{A}{l^2}$ is the aspect ratio of the interconnect [14]. Planar manufacturing techniques used in PCB and integrated circuit manufacturing lead to small aspect ratios because of the long lengths compared to the conductor width or height. Figure 1.1 displays the maximum bit rates over several orders of magnitudes of varying aspect ratios assuming a unity relation in Equation 1.5.

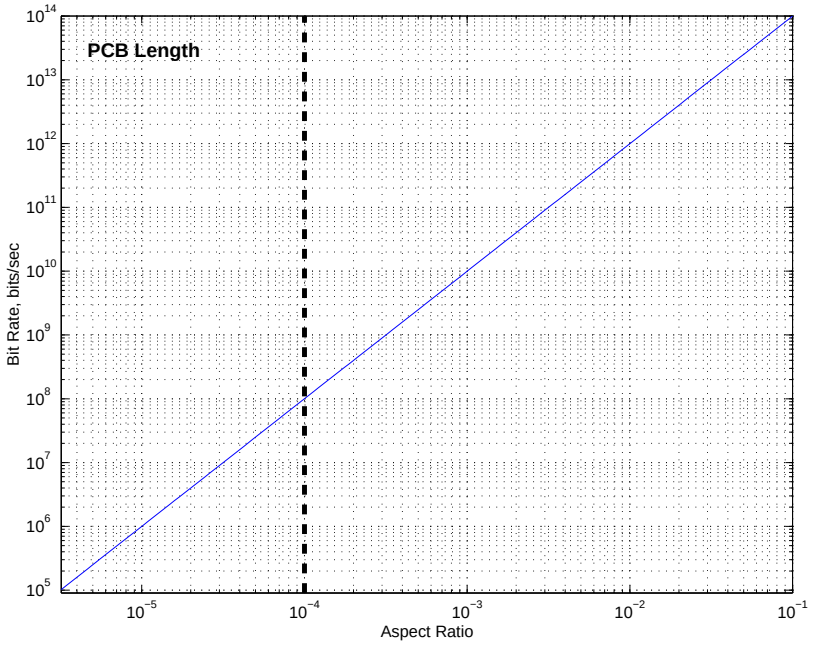

Figure 1.1: Effective Bit Rate of Electrical Interconnects of Various Aspect Ratios

The vertical line in Figure 1.1 is drawn where the aspect ratio equals 10^{-4}. This corresponds to a 25mil wide by 500mil long copper PCB trace fabricated with 1.0mil thick copper. Increasing the length of the line will cause the aspect ratio to fall below this limit in an inverse square manner.

Practical implementation issues, impedance mismatches for example, will have a detrimental effect on the channel and cause the realized bit rate to fall below the limit of Equation 1.5. Analysis methods such as scattering parameters introduced in Section 1.1.4 allow for the characterization of the channel to identify these effects.

1.1.2 Differential Signaling

Differential signaling is a signaling scheme where each bit is transmitted over two conductors. [9]. The data is transmitted by allowing a voltage difference to appear between the two conductors that make up the differential link. An example implementation may transmit a binary one value by placing the voltage at the source of conductor one, port one, to a preset value v_{high} while the voltage source of conductor two, port two, will be lowered to a preset value v_{low}. A binary zero value is transmitted by changing ports one and two to v_{low} and v_{high}, respectively.

The differential receiver tracks the relative voltage of conductor one, v_1, and conductor two, v_2 at ports three and four. The differential voltage is defined as,

$$v_{diff}(t) = v_1(t) - v_2(t), \tag{1.6}$$

while a common voltage is established by the average value of v_{low} and v_{high},

$$v_{common}(t) = \frac{1}{2}(v_1(t) + v_2(t)). \tag{1.7}$$

The differential design has several important advantages that allow for high speed links. The receiver tracks the relative differences in the signal while absolute voltage and current levels are ignored. The differential nature of the system provides inherent immunity to noise common to both conductors by removing any noise signal, $\eta(t)$, common to both conductors. Dynamic range of the received signal is increased by a factor of two compared to a single-ended system that uses the same voltage levels as the two conductors of the differential link individually swing through the same voltage range.

The design of a differential system is typically performed via a change of basis from a *nodal* space, where the voltage of each conductor is the basis used to describe the system, to a *modal* space where the common and differential voltages define the system. This change of basis is important because it allows design constrains such as the values of v_{common} and $|v_{diff}|$ to be defined in a basis that naturally flows from the design. Operating in the nodal space, these constraints must then be cast in terms of v_1 and v_2 whereas in the modal space these constraints can be used directly.

1.1.3 Multi-Bit Differential Signaling

Multiple parallel differential links can be used in parallel if the data rate of a single link is insufficient. For an n bit differential system, $2n$ interconnects are required. In some applications this can provide a restriction on the number of parallel differential links if the number of pins or required is more than can be provided. Current integrated circuit design practices dictate approximately one-half of the available pins of a semiconductor die to power and ground sources reducing the number of pins that can be used for the communications infrastructure.

Multi-bit differential signaling (MBDS) has been proposed as a solution to the area and pin drawbacks of differential systems. MBDS relies on an 'n choose m' or $C(n,m)$ coding scheme where m of the available n inputs and outputs are always guaranteed to be in a given state with the remaining $m-n$ in another unique state. A four choose two system is defined by requiring two of the four conductors to always be at a high voltage level, v_{high}, while the remaining two conductors are lowered to voltage level, v_{low}. This forms the set X where $X_{nm} = \{x_{nm} : x\varepsilon C\,(n,m)\}$. The number of elements ϕ in X_{nm} is given by,

$$\phi\{X_{nm}\} = \frac{n!}{(n-m)!m!}, \tag{1.8}$$

and is also known as the binomial coefficient $\binom{n}{m}$. The value of $\phi\{X_{nm}\}$ is maximized when n is $\frac{m}{2}$ where $\phi\{X_{n\lfloor\frac{n}{2}\rfloor}\} = \phi\{X_{n\lceil\frac{n}{2}\rceil}\}$. A classical differential system can be viewed as an MBDS system with a 'two choose one' or $C\,(2,1)$ code.

A direct implementation of an MBDS system will use a lookup table to directly map each element in X_{nm} to a binary value. When $\phi\{X_{nm}\}$ is not of two the number of effective bits the channel can carry with a one to one mapping of elements to binary values is,

$$bit_{eff} = \left\lfloor log_2\left(\frac{n!}{(n-m)!m!}\right)\right\rfloor. \tag{1.9}$$

Figure 1.2 shows how the effective bit width of MBDS links as a function of n grows where $n = \lfloor\frac{m}{2}\rfloor$. A $C\,(4,2)$ MBDS link has six unique codewords with the voltage levels of each conductor n at either v_{high} or v_{low}. The term *codeword* refers to each element of the set X_{nm} mapped onto the voltage levels v_{low} and v_{high}. The codeword $\{1,-1,-1,1\}$ defines conductors 1 and 4 at v_{high} while conductors 2 and 3 at v_{low}. The complete set of valid $C\,(4,2)$ codewords are shown

in Table 1.1. The rows of this table contains each codeword and it's *compliment*, defined as each codewords inverse mapping.

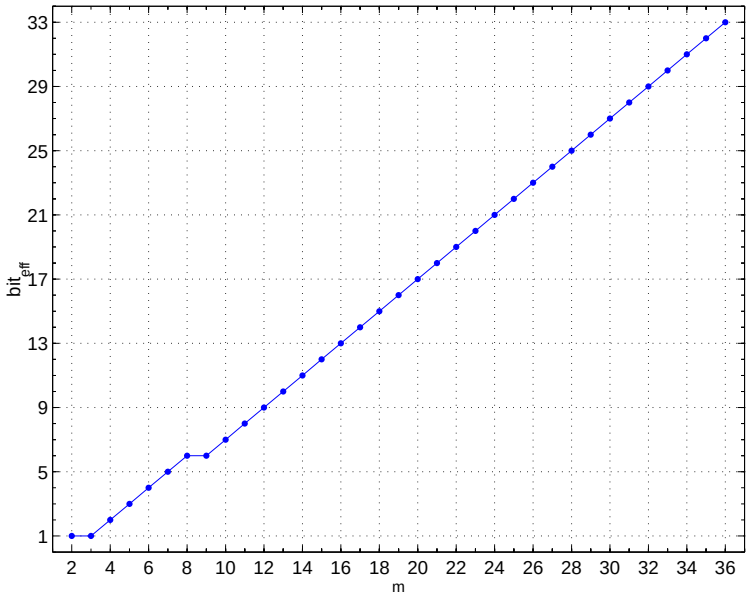

Figure 1.2: MBDS Effective Bit Width for $C(m, \lfloor \frac{m}{2} \rfloor)$.

Table 1.1: $C\,(4, 2)$ MBDS Codewords.

$\{1, 1, -1, -1\}$	$\{-1, -1, 1, 1\}$
$\{1, -1, 1, -1\}$	$\{-1, 1, -1, 1\}$
$\{1, -1, -1, 1\}$	$\{-1, 1, 1, -1\}$

Those codewords that are not partitioned into a representation of a binary value can then be used for other purposes as these extra codewords are free be used to signal other information such link control information. Bakos utilized these excess codewords to implement a lightweight hierarchical error control code over an MBDS link [1].

Extra codewords can also be used to match the characteristics of the channel to the set of codewords transmitted over the channel. There are six possible codeword combinations in a $C\,(4, 2)$

link; a two bit binary input leaves two extra codewords that can be arbitrarily partitioned or excluded altogether. These extra codewords give the an extra degree of freedom to leverage against the design constraints of the system. If there is a subset of codewords that can be pruned from the code-set, then it becomes advantageous to identify those codewords that may not propagate through the channel as well as other codewords, depending on how the boundary condition presented by the codewords form the solution to the telegraphers equations. Currently there is no method by which to identify such a partitioning.

MBDS as a differential signaling scheme requires a reference voltage to determine the value of each element of the codeword. This reference is created by a star termination network shown in Figure 1.3. The locus of the star network is referred to as the *common node* and is the differential reference point that is used by the each receiver to compare the voltage level of a conductor to the common node. The voltage at the common node in a $C\left(4,2\right)$ system with each termination resistor being equal is given by Kirchoff's current and voltage laws as,

$$v_{common}\left(t\right)=\frac{1}{4}\left[v_{1}\left(t\right)+v_{2}\left(t\right)+v_{3}\left(t\right)+v_{4}\left(t\right)\right]. \tag{1.10}$$

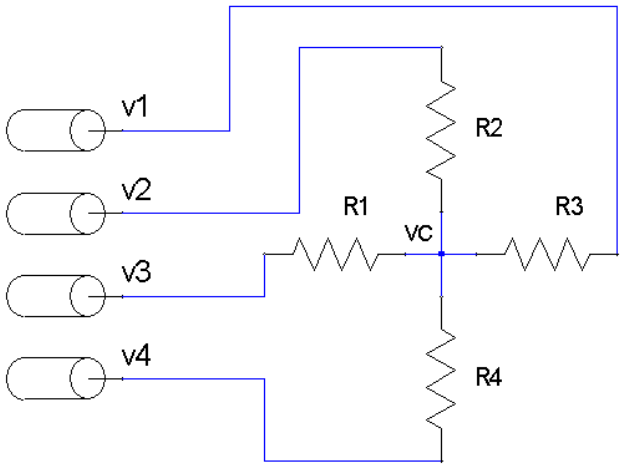

Figure 1.3: $C\left(4,2\right)$ Termination Network.

Any codeword that conforms to the MBDS $C\,(4,2)$ code-set will have the same common node voltage value establishing a fixed voltage reference. Global ground references for high speed signaling are usually not desirable as the drivers and receivers may not share the same common ground. This network also gives MBDS common mode noise rejection at the receiver inputs; interference such as electromagnetic interference that is injected into all members of the MBDS interconnect will be injected into the common node and removed by the comparators.

This work is partially motivated by the design possibilities that codeword selection MBDS gives to designers. The question becomes one of characterization, how to analyze the channel in a manner that is compatible with the restricted nature of MBDS systems. Current techniques such as scattering parameters are centered around a absolute frame of reference where each port is examined in terms of the the effect of a linear combination of the inputs to the system.

1.1.4 Scattering Parameters

Scattering parameters (S-parameters) are a linear network analysis tool for multi-port networks. Similar network analysis tools such as the impedance matrix (Z-network), admittance matrix (Y-network), or chain matrix (ABCD-network) all perform a linear mapping of input values to output values. The Z-network maps currents to voltages at each port of the network and are defined as,

$$\begin{bmatrix} v_1 \\ v_2 \\ \vdots \\ v_n \end{bmatrix} = \begin{bmatrix} Z_{11} & Z_{12} & \cdots & Z_{1n} \\ Z_{21} & Z_{22} & \cdots & Z_{2n} \\ \vdots & \vdots & \ddots & \vdots \\ Z_{n1} & Z_{n2} & \cdots & Z_{nn} \end{bmatrix} \begin{bmatrix} i_1 \\ i_2 \\ \vdots \\ i_n \end{bmatrix}, \tag{1.11}$$

or, in a matrix-vector notation [12],

$$\vec{\mathbf{v}} = \mathbf{Z}\vec{\mathbf{i}}. \tag{1.12}$$

These network descriptions are usually not used in high frequency RF applications where open and short circuit conditions are necessary at the ports in order to characterize the network. Open and short circuits will cause undesired reflections at frequencies where transmission line effects become dominate. These models also suffer from the inability to properly describe the effects

the termination of the network has on performance as each Z-matrix is uniquely defined for each termination network.

S-parameters are defined as the ratio of normalized *power waves* a_n to b_n. These power waves are defined at each port n as,

$$a_n = \frac{1}{2\sqrt{Z_{On}}} \left(v_n + Z_{On} i_n\right), \tag{1.13a}$$

$$b_n = \frac{1}{2\sqrt{Z_{On}}} \left(v_n - Z_{On} i_n\right), \tag{1.13b}$$

where n is the physical port terminated by impedance Z_{On} [11]. Solving Equations 1.13 for the port voltages and currents gives,

$$v_n = \sqrt{Z_{On}} \left(a_n + b_n\right), \tag{1.14a}$$

$$i_n = \frac{1}{\sqrt{Z_{On}}} \left(a_n - b_n\right). \tag{1.14b}$$

a_n and b_n are called power waves due to relation to the definition of power flowing into each port,

$$P_n = \frac{1}{2} Re\left[V_n I_n^*\right] = \frac{1}{2}\left[\left|a_n^2\right| - \left|b_n^2\right|\right], \tag{1.15}$$

where a_n represents the power wave flowing into port n and b_n is the power wave leaving the port.

In a transmission line the voltage and current waves at the ports are the summation of the forward and backward traveling waves,

$$v_n = v_n^+ + v_n^-, \tag{1.16a}$$

$$i_n = i_n^+ + i_n^-, \tag{1.16b}$$

allowing a_n and b_n to be rewritten as,

$$a_n = \frac{v_n^+}{\sqrt{Z_{On}}} = \sqrt{Z_{On}} i_n^+, \tag{1.17a}$$

$$b_n = \frac{v_n^-}{\sqrt{Z_{On}}} = -\sqrt{Z_{On}} i_n^-. \tag{1.17b}$$

S-parameters are defined as the fractional relation of the input power waves to the output power waves with,

$$S_{jk} = \left.\frac{b_j}{a_k}\right|_{a_{i\neq k}=0}, \tag{1.18}$$

where $a_{i\neq k} = 0$ implies that S_{jk} is the *response* at port j solely to the *stimulus* at port k. In vector notation,

$$\vec{\mathbf{b}} = \mathbf{S}\vec{\mathbf{a}}. \tag{1.19}$$

The purpose of the matrix $\mathbf{S}$ is to perform a linear mapping of the input stimulus vector $\vec{\mathbf{a}}$ to the stimulus response vector $\vec{\mathbf{b}}$. A two port device with stimulus waves a_1 and a_2 will have a response at port 1, b_1,

$$b_1 = S_{11}a_1 + S_{12}a_2. \tag{1.20}$$

Return loss is given by S_{11} and describes the fractional amount that a_1 is being reflected back to the source. The *insertion loss*, S_{12}, defines the attenuates of the power wave received at port two during propagation to port one.

Measuring S-parameters requires the conditions in Equation 1.18 to be satisfied. A two port device requires either a_1 or a_2 are guaranteed to be zero; these conditions require perfect impedance matching of the port to it's associated termination. At RF frequencies and higher S-parameters are preferred to other network descriptions as they can be measured without the use of short or open circuit conditions at the measurement ports.

1.2 PROBLEM STATEMENT

MBDS as a signaling technology retains the benefits of differential systems while reducing the number of pins required for parallel links. Currently there is no channel characterization technique available that allows an accurate quantification of the channel that the link will operate over in a manner that matches the stimulus present on the channel that conforms to MBDS codewords for any arbitrary $C\,(n, m)$ link. Current characterization techniques that exist are either on a port basis that gives no indication of the ensemble behavior of the system or are restricted to a classical differential, two-choose-one link.

Without this characterization, design classification of MBDS becomes difficult. Each $C(n, m)$ MBDS link will have n interconnects that must be routed through the PCB or backplane. Unlike the differential case where routing two coupled wires is limited to a few practical geometries, the interconnects in an MBDS link will be routed in a three dimensional structure with many possible configurations. Signal lines that are nearest neighbors may have more of coupling between each other than those signal lines at the periphery of the structure. The effects of this imbalance are unknown on the differential voltage and the common node voltage as seen at the output of the network.

The goal of this work is two fold; first to identify a means that will allow the characterization of MBDS channels and to survey practical PCB structures to determine layouts that have low loss for MBDS codewords or to identify those codewords that should be avoided in the MBDS code-set.

1.3 KEY CONTRIBUTIONS

Prior to this work, no method existed to allow the analysis of multi-bit differential channels. Design of PCB's for test implementations of MBDS circuitry had to be performed from a black box design perspective where the true impact of the channel on the behavior of the system was not understood. Chapter 3 introduces a method where a channel, such as a printed circuit board, can be characterized and the impact of the channel on the overall performance of the system can be understood.

Several PCB layouts are tested to determined the impact the topology of the PCB layout has on the performance of MBDS channels. These layouts are shown in Figures 4.1 and 4.2. Worst case scenario performance shows that in the case of the star geometry in the $C(6,3)$ case an unoptimized design can have a 10dB greater modal power loss than other structures.

This thesis also gives insight into the performance of multiple parallel differential links. Two differential channels that are close enough to each other such that they can no longer assume to be isolated, are subsets of the $C(4,2)$ MBDS code set. By performing the analysis presented here the impact of the proximity of the two channels can be analyzed.

2.0 PREVIOUS WORK

Scattering parameters have been in use by RF engineers for over fifty years. The ability to describe linear networks by power waves are extremely useful in circuit and RF design. Differential scattering parameters were rigorously developed as a theory when it became recognized that, in a differential system, references based on individual ports and a global ground reference are uninformative. Characterization of the design could not be carried out in a manner that fit the operating nature of the design.

2.1 DIFFERENTIAL SCATTERING PARAMETERS

Differential, mode specific scattering parameters were developed by Bockelman in 1995 to characterize differential systems in a frame of reference that naturally describes the system [3, 4, 7]. The specific motivation behind differential S-parameters was to develop a formulation that would allow for higher accuracy of on wafer differential structures.

Differential S-parameters in transmission line structures are uniquely adapted to the natural propagation of modes in a coupled transmission line structure. In this regime, a mode is defined as a solution to the transmission line equations outlined in Section 1.1.1. For a two conductor transmission line Equations 1.1 and 1.2 reduce to,

$$\begin{aligned}
\tfrac{d}{dx}v_1(z,t) &= -z_1 i_1(z)\, e^{j\omega t} - z_m i_2(z)\, e^{j\omega t} \\
\tfrac{d}{dx}v_2(z,t) &= -z_m i_1(z)\, e^{j\omega t} - z_2 i_2(z)\, e^{j\omega t} \\
\tfrac{d}{dx}i_1(z,t) &= -y_1 v_1(z)\, e^{j\omega t} - y_m v_2(z)\, e^{j\omega t} \\
\tfrac{d}{dx}i_2(x,t) &= -y_m v_1(z)\, e^{j\omega t} - y_2 v_2(z)\, e^{j\omega t},
\end{aligned} \tag{2.1}$$

where z_1, z_2, y_1 and y_2 are the self impedances and admittances per unit length while z_m and y_m define the mutual impedances and admittances. The $e^{j\omega t}$ harmonic time dependence will be furthermore suppressed while the frequency dependence of all coupling variables $z_n(\omega)$ and $y_n(\omega)$ are not treated in this analysis.

Closed form solutions to these equations have been published by Tripathi [16],

$$
\begin{aligned}
v_1(z) &= A_1 e^{-\gamma_c z} + A_2 e^{\gamma_c z} + A_3 e^{-\gamma_\pi z} + A_4 e^{\gamma_\pi z} \\
v_2(z) &= A_1 R_c e^{-\gamma_c z} + A_2 R_c e^{\gamma_c z} + A_3 R_\pi e^{-\gamma_\pi z} + A_4 R_\pi e^{\gamma_\pi z} \\
i_1(z) &= \tfrac{A_1}{Z_{c1}} e^{-\gamma_c z} - \tfrac{A_2}{Z_{c2}} e^{\gamma_c z} + \tfrac{A_3}{Z_{\pi 1}} e^{-\gamma_\pi z} - \tfrac{A_4}{Z_{\pi 2}} e^{\gamma_\pi z} \\
i_2(z) &= \tfrac{A_1 R_c}{Z_{c1}} e^{-\gamma_c z} - \tfrac{A_2 R_c}{Z_{c2}} e^{\gamma_c z} + \tfrac{A_3 R_\pi}{Z_{\pi 1}} e^{-\gamma_\pi z} - \tfrac{A_4 R_\pi}{Z_{\pi 2}} e^{\gamma_\pi z},
\end{aligned}
\tag{2.2}
$$

where $R_\pi = \frac{v_2}{v_1}$ and $R_c = \frac{v_2}{v_1}$ and the propagation constant, γ, defined as,

$$
\gamma_{c,\pi}^2 = \frac{y_1 z_1 + y_2 z_2}{2} + y_m z m \pm \frac{1}{2}\sqrt{(y_1 z_1 - y_2 z_2)^2 + 4(z_1 y_m + y_2 z_m)(z_2 y_m + y_1 z_m)}. \tag{2.3}
$$

π and c are defined as *modes of propagation* and define the two propagating voltage and current waves that propagate internally in the structure as solutions to Equation 2.1. A linear combination of these modes given in Equation 2.2 transform the modes into the nodal equivalent.

Assuming that the lines are symmetric Cohn provided a formulation and terminology such that the π and c modes reduce to even and odd modes of propagation, e and o respectively [6]. Symmetric coupled lines imply that $R_c = 1$ and $R_\pi = -1$.

The even and odd modes of propagation are analogous to Equations 1.6 and 1.7. The even mode of propagation occurs when the two conductors are at the same potential while currents in the conductors traveling in the same direction. Odd mode propagation requires that the conductors be at different potentials and the currents traveling in different directions. The characteristic impedance defined in Equation 2.2 causes $Z_e = Z_c$ and $Z_o = Z_\pi$.

The definition of common and differential modes versus even and odd are not always the same. Even and common modes are only equivalent under the conditions of a symmetric transmission line; the same relationship is valid for odd and differential modes. For other scenarios where the system is not subject to the symmetric constraint, this direct relationship may no longer be valid. Differential and common modes are defined as those modes that impinge upon the system from

external sources while even and odd modes are those modes that propagate internally as solutions to Equations 2.1.

Differential and common mode voltages are defined as,

$$v_d(z) = v_1(z) - v_2(z), \tag{2.4a}$$

$$v_c(z) = \frac{1}{2}(v_1 + v_2). \tag{2.4b}$$

The definition of differential current is dependent on the realization that the current entering a port equals the current returning on the other port requiring each port to sink one-half the difference between the two ports. The common mode current is the sum of the current entering the terminals of the transmission line. The differential and common mode currents are defined as,

$$i_d(z) = \frac{1}{2}(i_1 - i_2), \tag{2.5a}$$

$$i_c(z) = i_1(z) + i_2(z). \tag{2.5b}$$

In order to define differential S-parameters, expressions for differential voltage and currents are necessary and have been derived. The only remaining parameter to derive is the characteristic impedance of of each mode. Substituting the solutions to the transmission lines in Equation 2.2 into Equations 2.4 and 2.5 the characteristic impedance of each differential mode is simply the ratio of the forward traveling voltage waves to the forward traveling current waves of each propagation mode as follows,

$$z_d = 2Z_o, \tag{2.6a}$$

$$z_c = \frac{Z_e}{2}, \tag{2.6b}$$

where z_o and z_e are the characteristic impedances of the odd and even mode of propagation, respectively.

These definitions of the differential and common mode characteristic impedance can be used directly in the definition of differential S-parameters. Practical use of such a definition is not easily achieved as the termination of each differential mode is then different with both of these mode themselves different from the standard port impedances of most test equipment of 50Ω. For convenience and to maintain consistency with the vast array of test equipment in use it is required that

$Z_e = Z_o = Z_O$ where Z_O is the characteristic impedance of an uncoupled reference transmission line. Alternative definitions of differential impedance are valid, however the relationship between differential and standard S-parameters will change.

The requirement that $Z_e = Z_o = Z_O$ is a special solution to Equation 2.1 that forces all y_m and z_m to be equal to zero. In this regime, there is no coupling between the conductors of the transmission lines; each line is coupling only with the ground reference. This choice may seem overly simplistic and restrictive as well as contrary to the goal of differential S-parameters. This is resolved by the realization that Z_O in Equations 1.13 are the external terminations of the network and are not the characteristic impedance of the network itself. This defines the reference plane by which the multi-modal S-parameters are measured as uncoupled transmission lines.

Correct measurements of S-parameters must be performed under conditions of perfect matching, usually with a coaxial cable that satisfies the transmission line Equations 1.1 and 1.2 but has no coupling; i.e., $Z_e = Z_o = Z_O$, the exact case differential S-parameters are targeting. To interface a network to testing equipment the parameters need to be developed under the conditions that allow such testing. The statement that S-parameters can only be determined under conditions of perfect matching to to be interpreted as a testing condition only. Once the S-matrix has been characterized, it can then be renormalized under different termination conditions that will then describe the network under those conditions [15]. This is a useful feature of S-parameters; the effects of mismatched terminations can be observed.

2.1.1 Differential and Normal Scattering Parameter Relationships

Armed with proper definitions of differential mode voltages, currents and characteristic impedances, the definition of scattering parameters are identical in the differential case as in the nodal case and are defined by,

$$a_{mm}(z) = \frac{1}{2\sqrt{z_{mm}}}\left(v_{mm} + z_{mm} i_{mm}\right)\Big|_{z=0,l}, \tag{2.7a}$$

$$b_{mm}(z) = \frac{1}{2\sqrt{z_{mm}}}\left(v_{mm} - z_{mm} i_{mm}\right)\Big|_{z=0,l}, \tag{2.7b}$$

where mm is used to indicate the operation in the modal definition and not in standard nodal definition. Differential S-parameters will be defined as multi-modal S-parameters, $\mathbf{S}_{mm}$, while the normal frame of reference will be defined as nodal S-parameters, $\mathbf{S}_n$.

Port references undergo a new meaning in the differential case. A differential transmission line in the traditional sense can be viewed as a four port device. Under the differential S-parameter view the physical ports are reduced to two with port one corresponding to $z = 0$ and port two located at $z = l$. Each port is impinged upon with two different modes of stimulus: a_d the differential mode and a_c, the common mode. The S-parameter matrix under the differential formulation then becomes,

$$\vec{\mathbf{b}}_{mm} = \mathbf{S}_{mm}\vec{\mathbf{a}}_{mm}, \tag{2.8}$$

where each element of $\mathbf{S}_{mm}$, $S_{m_b m_a p_b p_a}$, refers to the response mode m_b measured at port p_b as a result of the stimulus of mode m_a at port p_a. For example, S_{dc21} implies the multi-modal S-parameter where physical port 1 is stimulated with a common mode signal with the measured differential mode response at port 2.

The direct relationship between $\mathbf{S}_n$ and $\mathbf{S}_{mm}$ is developed by replacing our definitions of v_d, v_c, i_d, i_c, z_d and z_c with there nodal equivalents as shown in the case of a_{d1},

$$\begin{aligned} a_{d1} &= \tfrac{1}{2\sqrt{z_d}}\left[v_{d1} + z_d i_d\right] \\ &= \tfrac{1}{2\sqrt{2Z_O}}\left[(v_1 - v_2) + 2Z_O\tfrac{1}{2}(i_1 - i_2)\right] \\ &= \tfrac{1}{\sqrt{2}}\left[\tfrac{1}{2\sqrt{Z_O}}(v_1 - v_2) - Z_O(i_1 - i_2)\right] \\ &= \tfrac{1}{\sqrt{2}}(a_1 - a_2). \end{aligned} \tag{2.9}$$

The same relationships for all stimulus and response modes at both ports are defined as,

$$\begin{aligned} a_{d1} &= \tfrac{1}{\sqrt{2}}(a_1 - a_2) \quad a_{d2} = \tfrac{1}{\sqrt{2}}(a_3 - a_4) \\ a_{c1} &= \tfrac{1}{\sqrt{2}}(a_1 + a_2) \quad a_{c2} = \tfrac{1}{\sqrt{2}}(a_3 + a_4) \\ b_{d1} &= \tfrac{1}{\sqrt{2}}(b_1 - b_2) \quad b_{d2} = \tfrac{1}{\sqrt{2}}(b_3 - b_4) \\ b_{c1} &= \tfrac{1}{\sqrt{2}}(b_1 + b_2) \quad b_{c2} = \tfrac{1}{\sqrt{2}}(b_3 + b_4). \end{aligned} \tag{2.10}$$

Observation of these results leads to a direct relationship between $\vec{\mathbf{a}}_n$ and $\vec{\mathbf{a}}_{mm}$,

$$\begin{bmatrix} a_{d1} \\ a_{d2} \\ a_{c1} \\ a_{c2} \end{bmatrix} = \frac{1}{\sqrt{2}} \begin{bmatrix} 1 & -1 & 0 & 0 \\ 0 & 0 & 1 & -1 \\ 1 & 1 & 0 & 0 \\ 0 & 0 & 1 & 1 \end{bmatrix} \begin{bmatrix} a_1 \\ a_2 \\ a_3 \\ a_4 \end{bmatrix}. \tag{2.11}$$

An equivalent transform is defined for $\vec{\mathbf{b}}_{mm}$ from $\vec{\mathbf{b}}_n$. Rewritten in a vector matrix notation,

$$\vec{\mathbf{a}}_{mm} = \mathbf{M}\vec{\mathbf{a}}_n, \tag{2.12}$$

where $\mathbf{M}$ is defined in Equation 2.11. Using the definition of S-parameters in the nodal and differential mode case from Equations 1.19 and 2.8 a direct relationship between $\mathbf{S_n}$ and $\mathbf{S_{mm}}$ is derived as,

$$\begin{aligned} \vec{\mathbf{b}}_{mm} &= \mathbf{S}_{mm}\vec{\mathbf{a}}_{mm} \\ \vec{\mathbf{b}}_{mm} = \mathbf{M}\vec{\mathbf{b}}_n \quad \vec{\mathbf{a}}_{mm} &= \mathbf{M}\vec{\mathbf{a}}_n \\ \mathbf{M}\vec{\mathbf{b}}_{mm} &= \mathbf{S}_{mm}\mathbf{M}\vec{\mathbf{a}}_{mm} \\ \vec{\mathbf{b}}_n &= \underbrace{\mathbf{M}^{-1}\mathbf{S}_{mm}\mathbf{M}}_{\mathbf{S}_n}\vec{\mathbf{a}}_n, \end{aligned} \tag{2.13}$$

using this last result gives relationships between $\mathbf{S_n}$ and $\mathbf{S_{mm}}$,

$$\mathbf{S_n} = \mathbf{M}^{-1}\mathbf{S_{mm}}\mathbf{M}, \tag{2.14a}$$

$$\mathbf{S_{mm}} = \mathbf{M}\mathbf{S_n}\mathbf{M}^{-1}. \tag{2.14b}$$

Equations 2.14a and 2.14b shows that $\mathbf{S}_{mm}$ is a linear transform of $\mathbf{S}_n$ by mapping $\vec{\mathbf{a}}_n$ and $\vec{\mathbf{b}}_n$ to the new basis vectors defined for differential voltages and currents. The transformation matrix $\mathbf{M}$ can be shown to be a unitary operator via the definition of such operators,

$$\mathbf{M}\mathbf{M}^{*T} = \mathbf{I}, \tag{2.15}$$

where $\mathbf{I}$ is the identity matrix. Because of unitary nature of $\mathbf{M}$ the nodal and the modal space are entirely equivalent and uniquely describe the same physical system with power in both spaces being conserved.

3.0 MBDS MODAL SCATTERING PARAMETERS

MBDS scattering parameters will be defined in a manner similar to differential S-parameters defined in Chapter 2. A slight but important distinction must be made comparing MBDS and differential S-parameters. When discussing differential transmission lines, the concept of modal solutions can be inferred directly from the solutions to the transmission line equations. Differential, or two-choose-one in MBDS definition, has two modes of signal propagation, two codewords, $\{1, -1\}$ and $\{-1, 1\}$, being transmitted on two conductors.

For any $C\left(m, n\right)$ system, there will be m conductors but the number of codewords, or driven modes, will be related to Equation 1.8. Modes that propagate internally in the transmission lines will be referred to as solution modes while MBDS modes will be referred to as driven modes. The term modal can either refer to solution modes or MBDS modes with the exact meaning dependent on context. Systems that are based on traditional per-port references will be referred to as nodal systems. The $C\left(2, 1\right)$ will continue to be referred to as differential to maintain parity with previously published work.

3.1 FOUR CHOOSE TWO MODAL S-PARAMETER DERIVATION

The currents and voltages of the four driven modes modes of propagation in the $C\left(4, 2\right)$ case will now be defined. Referring to Section 1.1.1, the transmission line equations are,

$$\begin{aligned} -\tfrac{d^2}{dz^2}\vec{\mathbf{V}} &= \mathbf{ZY}\vec{\mathbf{V}}, \\ -\tfrac{d^2}{dz^2}\vec{\mathbf{I}} &= \mathbf{YZ}\vec{\mathbf{I}}, \end{aligned} \tag{3.1}$$

where the $e^{j\omega t}$ is implicit, $\vec{\mathbf{V}}$ and $\vec{\mathbf{I}}$ are four element vectors, $\mathbf{Z}$ and $\mathbf{Y}$ are 4×4 element matrices. Closed form solutions to these coupled equations have not been published. Numerical solutions such as modal decomposition exist whereby the matrix $\mathbf{ZY}$ is diagonalized by a linear transform into a solution space where the differential equations become trivial to solve [8]. The method utilized in Section 2.1 as the solution to Equations 2.1 is an implementation of this technique for two-wire transmission lines.

To develop a consistent formulation, it will be assumed that the matrix $\mathbf{ZY}$ is diagonalized, i.e., there is no coupling in the transmission lines. This will define reference plane at the ports of the network under test as uncoupled transmission lines. The network under test becomes a 'black box' that distorts the voltage and currents seen by the reference transmission lines.

Equation 3.1 can be solved with the above simplifying condition for the propagating voltage waves from the reference plane,

$$\begin{aligned} v_1(z) &= v_1^+ e^{-\gamma_1 z} + v_1^- e^{\gamma_1 z} \\ v_2(z) &= v_2^+ e^{-\gamma_2 z} + v_2^- e^{\gamma_2 z} \\ v_3(z) &= v_3^+ e^{-\gamma_3 z} + v_3^- e^{\gamma_3 z} \\ v_4(z) &= v_4^+ e^{-\gamma_4 z} + v_4^- e^{\gamma_4 z}, \end{aligned} \tag{3.2}$$

where $v^{+,-}$ is the amplitude of the forward and backward traveling voltage wave and γ is the propagation constant for each line. An equivalent solution exists for the current,

$$\begin{aligned} i_1(z) &= i_1^+ e^{-\gamma_1 z} + i_1^- e^{\gamma_1 z} \\ i_2(z) &= i_2^+ e^{-\gamma_2 z} + i_2^- e^{\gamma_2 z} \\ i_3(z) &= i_3^+ e^{-\gamma_3 z} + i_3^- e^{\gamma_3 z} \\ i_4(z) &= i_4^+ e^{-\gamma_4 z} + i_4^- e^{\gamma_4 z}, \end{aligned} \tag{3.3}$$

with the same variable definitions for the voltage waves.

MBDS driven modes will now be defined. A $C(4,2)$ link has six valid codewords as defined in Table 1.1. A possible for MBDS modes could include defining six differential modes, one for each codeword, plus one common mode describing the common potential and current of each conductor. It is unnecessary to include each codewords with it's associated complement as the pair represent

the same information. The two codewords in the differential case, $\{1,-1\}$ and $\{-1,1\}$, have the voltage and current definition from Equations 2.4 and 2.5,

$$\begin{aligned} v_{d_{\{1,-1\}}} &= v_1 - v_2 = -\left(v_2 - v_1\right) = -v_{d_{\{-1,1\}}} \\ i_{d_{\{1,-1\}}} &= \tfrac{1}{2}\left(i_1 - i_2\right) = -\tfrac{1}{2}\left(i_2 - i_1\right) - i_{d_{\{-1,1\}}}. \end{aligned} \tag{3.4}$$

Substituting the voltage definitions for the two codewords in Equation 2.7a, the definition of a_{mm} gives the result,

$$a_{d_{\{-1,1\}}} = \frac{1}{\sqrt{2}}\left(a_2 - a_1\right) = -a_{d_{\{1,-1\}}}, \tag{3.5}$$

and contains the same power wave information; the sign change indicates that the 'direction' of the mode has been reversed.

$C(4,2)$ modes will be defined by parsing the code-set to remove complements and defining the three differential modes and one common mode similar to Equations 2.4 and 2.5. The voltage of each mode is defined as,

$$\begin{aligned} v_{m_1} &= v_1 + v_2 - v_3 - v_4 \\ v_{m_2} &= v_1 - v_2 + v_3 - v_4 \\ v_{m_3} &= v_1 - v_2 - v_3 + v_4 \\ v_{m_c} &= \tfrac{1}{4}\left(v_1 + v_2 + v_3 + v_4\right), \end{aligned} \tag{3.6}$$

and the modal current definition is defined by,

$$\begin{aligned} i_{m_1} &= \tfrac{1}{4}\left(i_1 + i_2 - i_3 - i_4\right) \\ i_{m_2} &= \tfrac{1}{4}\left(i_1 - i_2 + i_3 - i_4\right) \\ i_{m_3} &= \tfrac{1}{4}\left(i_1 - i_2 - i_3 + i_4\right) \\ i_{m_c} &= i_1 + i_2 + i_3 + i_4. \end{aligned} \tag{3.7}$$

Given the definitions for modal current and voltage, a definition for impedance can be devolved. Substituting the definition of the forward traveling modal voltage for v_{m_1} in Equation 3.2,

$$v^+_{m_1}(z) = v^+_1 e^{-\gamma_1 z} + v^+_2 e^{-\gamma_2 z} - v^+_3 e^{-\gamma_3 z} - v^+_4 e^{-\gamma_4 z}. \tag{3.8}$$

The current is defined by the definition of characteristic impedance as the ratio of the traveling voltage and current wave of each line n and the modal current definition given in Equation 3.3,

$$i^+_{m_1}(z) = \frac{1}{4}\left(\frac{v^+_1}{Z_{O_1}}e^{-\gamma_1 z} + \frac{v^+_2}{Z_{O_2}}e^{-\gamma_2 z} + \frac{v^+_3}{Z_{O_3}}e^{-\gamma_3 z} - \frac{v^+_4}{Z_{O_4}}e^{-\gamma_4 z}\right). \tag{3.9}$$

The reference plane is assumed to be balanced where $Z_{O_1} = Z_{O_2} = Z_{O_3} = Z_{O_4} = Z_O$. Under this condition the modal impedance z_{m_1} is determined as,

$$z_{m_1} = \frac{v^+_{m_1}}{i^+_{m_1}} = 4Z_O. \tag{3.10}$$

Voltage and current waves for the remaining modes follow the same derivation. Impedance definitions for all modes can be determined as,

$$z_{m_1} = z_{m_2} = z_{m_3} = 4Z_O, \tag{3.11a}$$

$$z_{m_c} = \frac{Z_O}{4}. \tag{3.11b}$$

Comparing Equation 2.6 with Equations 3.11 implies that that the $C(4,2)$ network is simply an extension of the differential case.

3.1.1 Modal and Nodal S-Parameter Relationship

Port definitions will retain the semantics introduced in Section 2.1.1 with the extension that there are now three differential modes. a_{mm} and b_{mm} power waves can now be defined using the definition of $C(4,2)$ modal currents, voltages and impedances. $a_{m_1,1}$, the application of i_{m_1} and v_{m_1} at $z = 0$, is defined as,

$$\begin{aligned} a_{m_1 1} &= \tfrac{1}{2\sqrt{z_{m_1}}}\left[v_{m_1} - z_{m_1} i_{m_1}\right] \\ &= \tfrac{1}{2\sqrt{4Z_O}}\left[v_1 + v_2 - v_3 - v_4 + \tfrac{4Z_O}{4}\left(i_1 + i_2 - i_3 - i_4\right)\right] \\ &= \tfrac{1}{4\sqrt{Z_O}}\left[v_1 - Z_0 i_1 + v_2 - Z_0 i_2 - v_3 + Z_0 i_3 - v_4 + Z_0 i_4\right] \\ &= \tfrac{1}{2}\left[a_1 + a_2 - a_3 - a_4\right]. \end{aligned} \tag{3.12}$$

Similar derivations can be made for all a_{mm} and b_{mm} from the nodal frame of reference are defined as,

$$
\begin{aligned}
a_{m_1 1} &= \tfrac{1}{2}\left[a_1 + a_2 - a_3 - a_4\right] & a_{m_1 2} &= \tfrac{1}{2}\left[a_5 + a_6 - a_7 - a_8\right] \\
a_{m_2 1} &= \tfrac{1}{2}\left[a_1 - a_2 + a_3 - a_4\right] & a_{m_2,2} &= \tfrac{1}{2}\left[a_5 - a_6 + a_7 - a_8\right] \\
a_{m_3 1} &= \tfrac{1}{2}\left[a_1 - a_2 - a_3 + a_4\right] & a_{m_3 2} &= \tfrac{1}{2}\left[a_5 - a_6 - a_7 a + a_8\right] \\
a_{m_c 1} &= \tfrac{1}{2}\left[a_1 + a_2 - a_3 - a_4\right] & a_{m_1 2} &= \tfrac{1}{2}\left[a_5 + a_6 - a_7 - a_8\right] \\
b_{m_1 1} &= \tfrac{1}{2}\left[b_1 + b_2 - b_3 - b_4\right] & b_{m_1 2} &= \tfrac{1}{2}\left[b_5 + b_6 - b_7 - b_8\right] \\
b_{m_2 1} &= \tfrac{1}{2}\left[b_1 - b_2 + b_3 - b_4\right] & b_{m_2 2} &= \tfrac{1}{2}\left[b_5 - b_6 + b_7 - b_8\right] \\
b_{m_3 1} &= \tfrac{1}{2}\left[b_1 - b_2 - b_3 + b_4\right] & b_{m_3 2} &= \tfrac{1}{2}\left[b_5 - b_6 - b_7 + b_8\right] \\
b_{m_c 1} &= \tfrac{1}{2}\left[b_1 + b_2 - b_3 - b_4\right] & b_{m_1 2} &= \tfrac{1}{2}\left[b_5 + b_6 - b_7 - b_8\right].
\end{aligned}
\tag{3.13}
$$

Converting between $\mathbf{S}_{mm}$ and $\mathbf{S}_n$ can be performed in the same manner as in Equation 2.11,

$$
\begin{bmatrix} a_{m_1 1} \\ a_{m_1 2} \\ a_{m_2 1} \\ a_{m_2 2} \\ a_{m_3 1} \\ a_{m_3 2} \\ a_{m_c 1} \\ a_{m_c 2} \end{bmatrix}
= \frac{1}{2}
\begin{bmatrix}
1 & 1 & -1 & -1 & 0 & 0 & 0 & 0 \\
0 & 0 & 0 & 0 & 1 & 1 & -1 & -1 \\
1 & -1 & 1 & -1 & 0 & 0 & 0 & 0 \\
0 & 0 & 0 & 0 & 1 & -1 & 1 & -1 \\
1 & -1 & -1 & 1 & 0 & 0 & 0 & 0 \\
0 & 0 & 0 & 0 & 1 & -1 & -1 & 1 \\
1 & 1 & 1 & 1 & 0 & 0 & 0 & 0 \\
0 & 0 & 0 & 0 & 1 & 1 & 1 & 1
\end{bmatrix}
\begin{bmatrix} a_1 \\ a_2 \\ a_3 \\ a_4 \\ a_5 \\ a_6 \\ a_7 \\ a_8 \end{bmatrix}.
\tag{3.14}
$$

A equivalent definition exists for $\vec{\mathbf{b}}_{mm}$. Following the derivation of Equation 2.13, a linear transform can be defined from $\mathbf{S}_n$ to $\mathbf{S}_{mm}$ and vice versa by,

$$
\mathbf{S}_n = \mathbf{M}^{-1}\mathbf{S}_{mm}\mathbf{M}, \tag{3.15}
$$

$$
\mathbf{S}_{mm} = \mathbf{M}\mathbf{S}_n\mathbf{M}^{-1}, \tag{3.16}
$$

where M is defined in Equation 3.14. The matrix $\mathbf{M}$ is a linear operator that maps $\mathbf{S}_n$ to $\mathbf{S}_{mm}$ and obeys the properties of such operators as defined in section 2.1.1.

3.2 SIX CHOOSE THREE MODAL S-PARAMETER DERIVATION

The $C(6,3)$ modal derivation is performed in a similar manner to the $C\,(4,2)$. The same assumptions used the $C(4,2)$ case are repeated; the reference plane will be uncoupled transmission lines at the ports of the network. The uncoupled assumption will allow us to define six-conductor transmission line equations for the voltage and current waves analogous to Equations 3.2 and 3.3.

A $C\,(6,3)$ link has twenty unique codewords. Parsing the code-set to remove equivalent compliments and adding our definition of a common mode analogous to Equations 3.6 and 3.7 the driven modal voltage on the transmission lines are,

$$\begin{bmatrix} v_{m_1}(z) \\ v_{m_2}(z) \\ v_{m_3}(z) \\ v_{m_4}(z) \\ v_{m_5}(z) \\ v_{m_5}(z) \\ v_{m_6}(z) \\ v_{m_7}(z) \\ v_{m_8}(z) \\ v_{m_9}(z) \\ v_{m_{10}}(z) \\ v_{m_c}(z) \end{bmatrix} = \begin{bmatrix} 1 & 1 & 1 & -1 & -1 & -1 \\ 1 & 1 & -1 & 1 & -1 & -1 \\ 1 & 1 & -1 & -1 & 1 & -1 \\ 1 & 1 & -1 & -1 & -1 & 1 \\ 1 & -1 & 1 & 1 & -1 & -1 \\ 1 & -1 & 1 & -1 & 1 & -1 \\ 1 & -1 & 1 & -1 & -1 & 1 \\ 1 & -1 & -1 & 1 & 1 & -1 \\ 1 & -1 & -1 & 1 & -1 & 1 \\ 1 & -1 & -1 & -1 & 1 & 1 \\ \frac{1}{6} & \frac{1}{6} & \frac{1}{6} & \frac{1}{6} & \frac{1}{6} & \frac{1}{6} \end{bmatrix} \begin{bmatrix} v_1(z) \\ v_2(z) \\ v_3(z) \\ v_4(z) \\ v_5(z) \\ v_6(z) \end{bmatrix}. \tag{3.17}$$

The equation for modal currents are defined in a similar manner to Equation 3.7 with the appropriate normalizing factor and will not be repeated here. Modal impedance for each mode is derived analogous to Equation 3.10 as,

$$\begin{aligned} z_{m_x} &= 6Z_O, \\ z_{m_c} &= \frac{Z_O}{6}. \end{aligned} \tag{3.18}$$

Using the definitions of modal voltage, impedance and current the relationship between $\vec{\mathbf{a}}_{mm}$ and $\vec{\mathbf{a}}_n$ is defined as,

(3.19)

$$\begin{bmatrix} a_{m_1,1} \\ a_{m_1,2} \\ a_{m_2,1} \\ a_{m_2,2} \\ a_{m_3,1} \\ a_{m_3,2} \\ a_{m_4,1} \\ a_{m_4,2} \\ a_{m_5,1} \\ a_{m_5,2} \\ a_{m_6,1} \\ a_{m_6,2} \\ a_{m_7,1} \\ a_{m_7,2} \\ a_{m_8,1} \\ a_{m_8,2} \\ a_{m_9,1} \\ a_{m_9,2} \\ a_{m_{10},1} \\ a_{m_{10},1} \\ a_{m_c,1} \\ a_{m_c,2} \end{bmatrix} = \frac{1}{\sqrt{6}} \begin{bmatrix} 1 & 1 & 1 & -1 & -1 & -1 & 0 & 0 & 0 & 0 & 0 & 0 \\ 0 & 0 & 0 & 0 & 0 & 0 & 1 & 1 & 1 & -1 & -1 & -1 \\ 1 & 1 & -1 & 1 & -1 & -1 & 0 & 0 & 0 & 0 & 0 & 0 \\ 0 & 0 & 0 & 0 & 0 & 0 & 1 & 1 & -1 & 1 & -1 & -1 \\ 1 & 1 & -1 & -1 & 1 & -1 & 0 & 0 & 0 & 0 & 0 & 0 \\ 0 & 0 & 0 & 0 & 0 & 0 & 1 & 1 & -1 & -1 & 1 & -1 \\ 1 & 1 & -1 & -1 & -1 & 1 & 0 & 0 & 0 & 0 & 0 & 0 \\ 0 & 0 & 0 & 0 & 0 & 0 & 1 & 1 & -1 & -1 & -1 & 1 \\ 1 & -1 & 1 & 1 & -1 & -1 & 0 & 0 & 0 & 0 & 0 & 0 \\ 0 & 0 & 0 & 0 & 0 & 0 & 1 & -1 & 1 & 1 & -1 & -1 \\ 1 & -1 & 1 & -1 & 1 & -1 & 0 & 0 & 0 & 0 & 0 & 0 \\ 0 & 0 & 0 & 0 & 0 & 0 & 1 & -1 & 1 & -1 & 1 & -1 \\ 1 & -1 & 1 & -1 & -1 & 1 & 0 & 0 & 0 & 0 & 0 & 0 \\ 0 & 0 & 0 & 0 & 0 & 0 & 1 & -1 & 1 & -1 & -1 & 1 \\ 1 & -1 & -1 & 1 & 1 & -1 & 0 & 0 & 0 & 0 & 0 & 0 \\ 0 & 0 & 0 & 0 & 0 & 0 & 1 & -1 & -1 & 1 & 1 & -1 \\ 1 & -1 & -1 & 1 & -1 & 1 & 0 & 0 & 0 & 0 & 0 & 0 \\ 0 & 0 & 0 & 0 & 0 & 0 & 1 & -1 & -1 & 1 & -1 & 1 \\ 1 & -1 & -1 & -1 & 1 & 1 & 0 & 0 & 0 & 0 & 0 & 0 \\ 1 & 1 & 1 & 1 & 1 & 1 & 0 & 0 & 0 & 0 & 0 & 0 \\ 0 & 0 & 0 & 0 & 0 & 0 & 1 & 1 & 1 & 1 & 1 & 1 \end{bmatrix} \begin{bmatrix} a_1 \\ a_2 \\ a_3 \\ a_4 \\ a_5 \\ a_6 \\ a_7 \\ a_8 \\ a_9 \\ a_{10} \\ a_{11} \\ a_{12} \end{bmatrix}.$$

An equivalent definition exists for $\vec{\mathbf{b}}_{mm}$ using the matrix $\mathbf{M}$ defined in Equation 3.19. Unlike the differential and $C\left(4,2\right)$ case, a linear transform between the nodal and modal basis can not be defined because the matrix $\mathbf{M}$ is not invertible. This is a consequence of the fact that $\mathbf{M}$ is not square. There is no unique linear mapping between the modal definitions and the nodal definitions as there are more modes than nodes. In the modal space, the nodal space becomes overdetermined.

This is not restricted to the $C(6,3)$ MBDS link. Any MBDS link that has does not have the same number of modes as conductors automatically falls into this situation. Since a linear transform can not be defined a direct relationship between $\mathbf{S}_n$ and $\mathbf{S}_{mm}$ can not be defined. Solutions such as a pseudo-inverse of the matrix $\mathbf{M}$ can be used to find a least-squares matrix that would provide a way to convert between the modal space and the nodal space but these methods are undesirable as there are many possible such solutions.

A numerical technique can be defined using the definitions of Equations 1.18 and 3.19. S-parameters are defined simply as a ratio between a_x and b_y and Equation 3.19 gives a way to move between $\vec{\mathbf{a}}_n$ and $\vec{\mathbf{a}}_{mm}$ as well as $\vec{\mathbf{b}}_n$ and $\vec{\mathbf{b}}_{mm}$.

To calculate multi-modal S-parameters it will be assumed that $\mathbf{S}_n$ is already known. The rows of the matrix $\mathbf{M}$ conform to proper MBDS codewords. This is not by accident and is the same for differential and for $C(4,2)$ multi-modal S-parameters in Equations 2.10 and 3.14. Using the rows of this matrix as an $\vec{\mathbf{a}}_{n_{mx}}$ vector, the response vector $\vec{\mathbf{b}}_{n_{mx}}$ can be calculated via $\mathbf{S}_n$. Once $\vec{\mathbf{b}}_{n_{mx}}$ is known it is converted to $\vec{\mathbf{b}}_{mm}$ via Equation 3.19 to give all the modal responses to the input mode $\vec{\mathbf{a}}_{n_{mx}}$. $\vec{\mathbf{a}}_{mm}$ is then calculated by following the definition in Equation 3.19. Because $\mathbf{M}$ is not a valid linear transform, non-zero modal terms will appear in the result vector $\vec{\mathbf{a}}_{mm}$. Because of this, each $\vec{\mathbf{a}}_{mm}$ must be calculated by using the appropriate input codeword otherwise power will not be conserved. Using the $\vec{\mathbf{b}}_{mm}$ and the a_{mm} the column of the $\mathbf{S}_{mm}$ matrix reserved for this stimulus can be calculated by applying the definition of S-parameters.

3.3 GENERALIZED MBDS MULTI-MODAL S-PARAMETERS

The $C(6,3)$ derivation provides a method whereby the number of differential modes is greater than the number of solutions to the transmission line equations. This will allow the characterization of any MBDS channel via S-parameter measurements.

Keeping parity with all situations presented so far, the consistent reference plane of uncoupled transmission lines will be assumed. The forward traveling voltage wave at the reference measurement plane for each reference conductor, i, is defined as,

$$v_i^+(z) = v_i^+ e^{-\gamma_i z}, \tag{3.20}$$

with the forward traveling current wave defined via,

$$i_i^+(z) = i_i^+ e^{-\gamma_i z}, \tag{3.21}$$

with the harmonic time dependence suppressed.

Using the definition of the reference plane of uncoupled transmission lines the modes for each MBDS link must be then be defined. The differential modes can be defined by parsing the set X_{nm} that contains the MBDS codewords to remove codewords that are complements. This will reduce the size of the set $\phi\{X_{nm}\}$, defined in Equation 1.8, by one half. The voltage definition of the differential modes is,

$$v_{m_x} = \sum_{i=1}^{m} k_i v_i, \tag{3.22}$$

where k_i are elements of each codeword y_{nm} in the set, $Y_{nm} = \{y_{nm} : y \varepsilon C(n,m), y_{nm} = \bar{y}_{nm}\}$. The modal current is defined as,

$$i_{m_x} = \frac{1}{m} \sum_{i=1}^{m} k_i i_i. \tag{3.23}$$

The common mode must also be added to the set of modal current and voltage definitions. They are defined as,

$$v_{m_c} = \frac{1}{m} \sum_{i=1}^{m} v_i, \tag{3.24a}$$

$$i_{m_c} = \sum_{i=1}^{m} i_i. \tag{3.24b}$$

Modal impedance is defined as,

$$z_{m_i} = m Z_O, \tag{3.25a}$$

$$z_{m_c} = \frac{Z_O}{m}, \tag{3.25b}$$

with the assumption that the structure under test is terminated with impedance Z_O at each physical port.

The power waves flowing into and out of the structure being tested can be determined by replacing the modal current, voltage and impedance definitions for each mode into the power wave equations. For multi-modal port one, $z = 0$, having nodal ports one through n,

$$\begin{aligned} a_{m_x,1} &= \frac{1}{2\sqrt{z_{m_x}}} \left[v_{m_x} - z_{m_x} i_{m_x} \right], \\ &= \frac{1}{\sqrt{m}} \left[\sum_{i=1}^{m} k_i a_i \right], \end{aligned} \tag{3.26}$$

with the definition for multi-modal port two equivalent with the replacement of a_i with a_{m+i}. The same definition exists for $b_{m_x,y}$.

These definitions allow us to write a relationship between $\vec{\mathbf{a}}_m$, $\vec{\mathbf{a}}_n$, $\vec{\mathbf{b}}_m$, and $\vec{\mathbf{b}}_n$ by defining a matrix $\mathbf{M}$ that will convert the nodal frame of reference into a modal solution. The rows of the matrix $\mathbf{M}$ are the members of the set Y_{nm} defined at physical ports one and two, with the common mode definition included, and multiplied by the normalizing factor $\frac{1}{\sqrt{m}}$.

Once $\mathbf{M}$ has been defined, the algorithm outlined in Section 3.2 can be applied to determine the $\mathbf{S}_{mm}$ matrix given the $\mathbf{S}_n$ matrix.

The $C\,(4, 2)$ MBDS S-parameters have the advantage that if either the nodal or the multi-modal S-matrix is known it can uniquely describe the multi-modal or nodal S-matrix. A multi-modal S-matrix can be directly characterized through the use of power splitters and baluns to generate the appropriate stimulus and measure the multi-modal response. Multi-modal characterization of other MBDS links can only be individually defined by an associated nodal S-matrix as each multi-modal S-matrix corresponds to an entire set of nodal S-parameters.

4.0 EXPERIMENTAL DESIGN

The methods defined in Chapter 3 were used to analyze several proposed PCB trace configurations of $C(4,2)$ and $C(6,3)$ MBDS links. A simulation design flow was developed and is complemented by the manufacture and characterization of the structures presented here. The analysis flow allows for the extraction of all nodal and multi-modal S-parameters.

Simulations were performed for three different basic geometries of trace configuration in a PCB for $C(4,2)$ and $C(6,3)$ links. The three chosen configurations included a planar layout where all traces were routed on the same PCB layer, a square geometry where the outline of the trace stack-up is rectangular in shape and a star geometry designed to present the most overall symmetric surroundings to each trace. These configurations are presented in Figures 4.1 and 4.2 for both the four choose two and the six choose three links. The trace numberings one through m correspond to nodal ports 1 one m and $m+1$ though $2m$, i.e., trace one in the $C(4,2)$ planar geometry identifies nodal ports one and five.

Simulations of each link configuration are performed by creating a model of a one-half inch section of PCB trace using *Ansoft HFSS* to create a high frequency, wide band model of the behavior of the electromagnetic field in the PCB. *Ansoft Designer* is used to combine the individual PCB sections into a single eight inch PCB model. Vias, connectors or other components are not simulated in this model. All transmission line structures are bounded on adjacent layers above and below of the model with ground planes. The nodal S-parameter matrix for the eight inch model is calculated in *Designer* with all measurement ports simulating a reference 50Ω termination impedance. The nodal S-Parameter matrix is then imported into *Matlab* and the multi-modal S-parameter matrix was calculated. The HFSS model was solved for frequencies up to 25GHz.

A test PCB with the same transmission line structures was manufactured on a six-layer manufacturing process with 1.0oz copper traces in each signal plane and FR-4 dielectric. To maintain

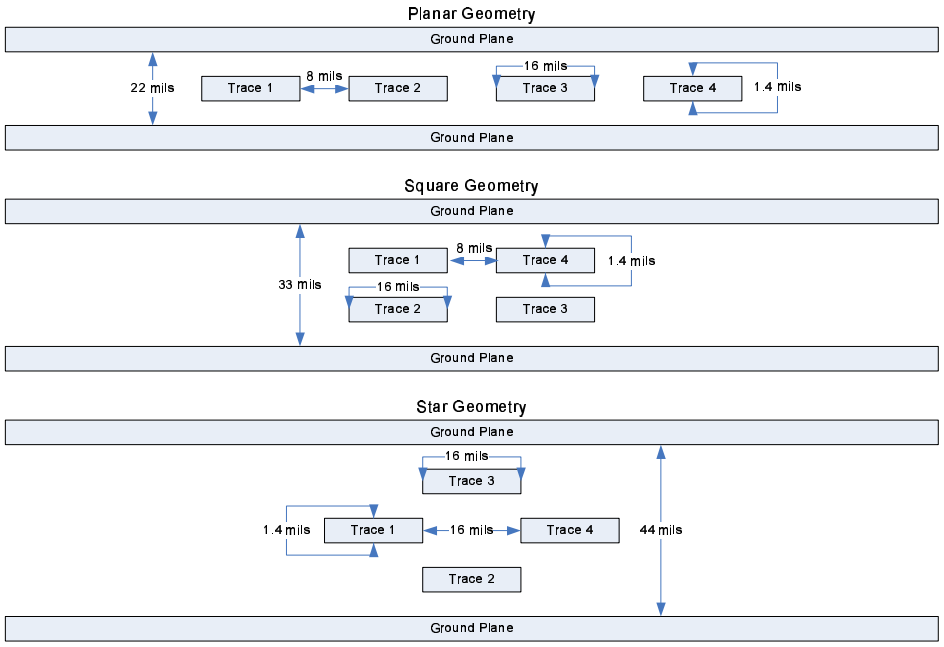

Figure 4.1: $C\,(4,2)$ Simulation and Test PCB Configurations.

parity with the simulations, a grounded plane bounds the upper and lower level of the traces. The PCB is analyzed with an Agilent Technologies 8712ET RF Network Analyzer in the range of 300KHz to 1.3GHz to collect the nodal S-parameter data. *Matlab* is used to generate the multi-modal S-parameters.

The goal of these experiments is to identify those structures that result in the lowest losses for MBDS modes. The design flow allows for the capture of all sixty-four $C\,(4,2)$ nodal and multi-modal S-parameters, the 144 nodal S-parameters and 484 multi-modal $C\,(6,3)$ S-parameters. This thesis will only concentrate on return loss, S_{xx} and $S_{m_x m_x 11}$, and insertion loss S-parameters,$S_{x(m+x)}$ and $S_{m_x m_x 21}$. Cross modal characteristics will not be presented here.

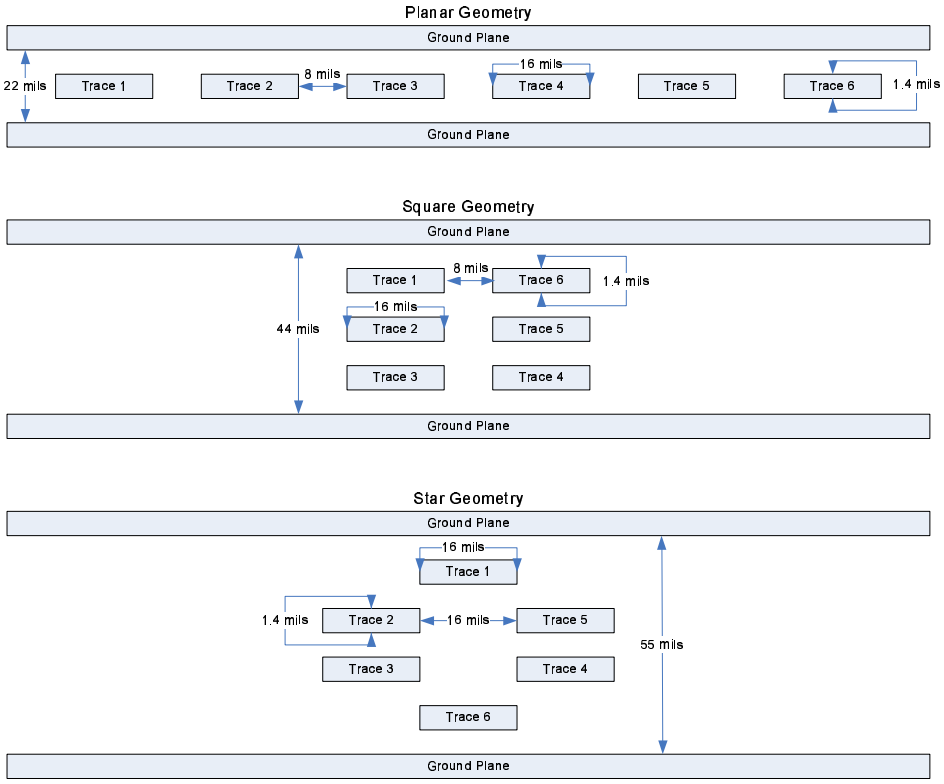

Figure 4.2: $C\,(6,3)$ Simulation and Test PCB Configurations.

5.0 EXPERIMENTAL RESULTS

5.1 FOUR CHOOSE TWO RESULTS

5.1.1 Planar Geometry

The results for the eight inch simulations and measured data for the $C\,(4,2)$ from 300kHz to 1.3GHz for the planar geometry are shown in Figures 5.1 and 5.2. The plots show the insertion loss and the return loss in both the nodal and multi-modal space over the frequency range from 300kHz to 1.3GHz.

Figure 5.1 shows the effects of the asymmetry created perpendicular to the plane of the PCB by the two traces that only have one neighbor giving different off diagonal terms in $\mathbf{ZY}$. The return loss in the nodal space of Figure 5.1a indicates that because of the asymmetry the inner two conductors in this configuration also have a different characteristic impedance and leads to higher return loss.

The degeneracy created by the different nodal responses is translated into the modal space as displayed in Figure 5.2. $S_{m_1m_121}$ displays a lower insertion loss than the other differential modes. This particular mode corresponds to codeword $\{1,1,-1,-1\}$ and creates an situation where the voltage and current waves split along the vertical axis of symmetry and both conductors on each side have the same potential and current direction and a different current and voltage relative to the mirror side. $S_{m_2m_221}$, corresponding to codeword $\{1,-1,1,-1\}$, has higher loss over the entire frequency range and at some frequencies is 1dB lower than $S_{m_1m_121}$. Electrostatic plots of the electric field of this geometry for S_{m_1} and S_{m_2} with a 100mV potential difference are shown in Figure 5.3.

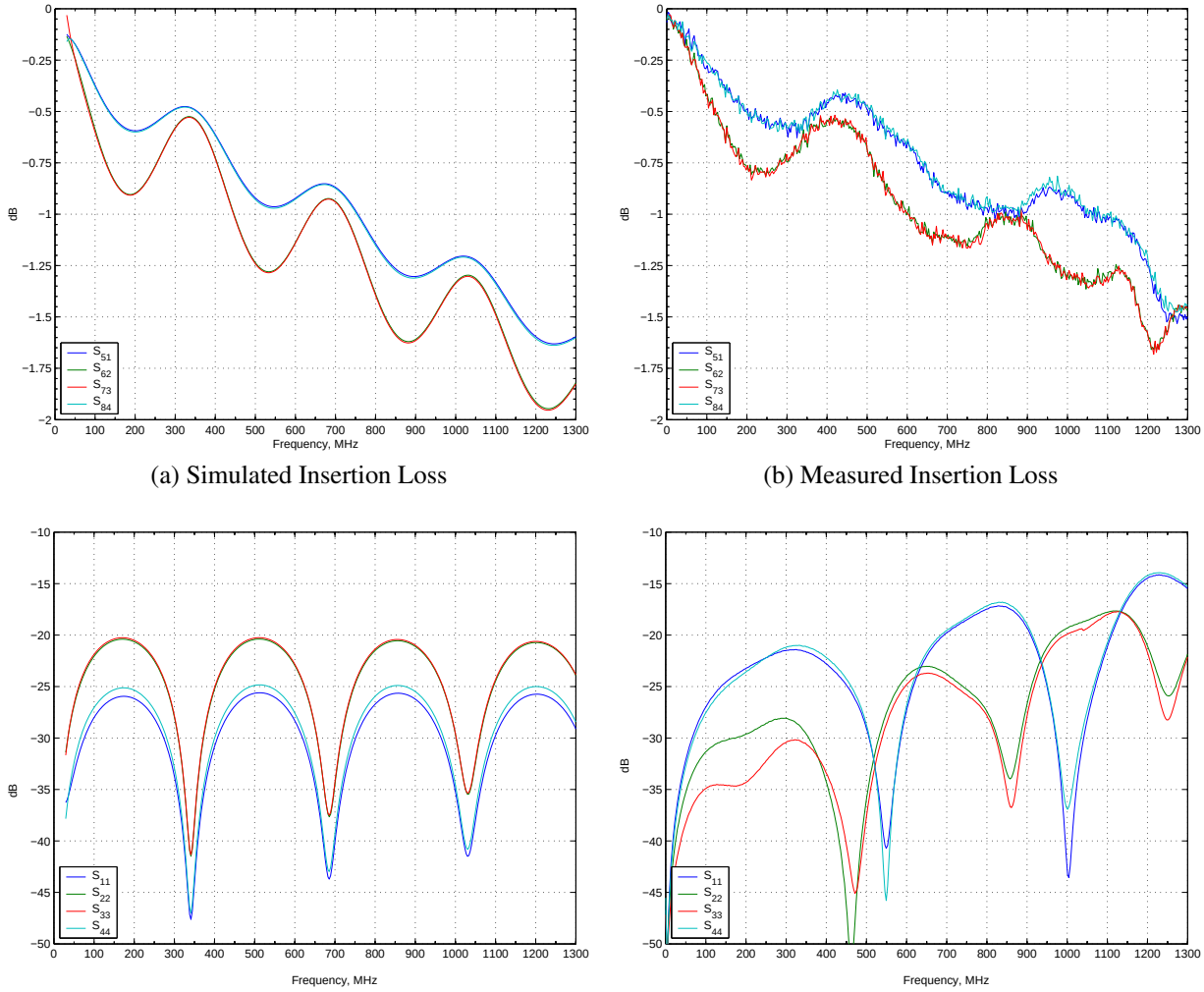

(a) Simulated Insertion Loss

(b) Measured Insertion Loss

(c) Simulated Return Loss

(d) Measured Return Loss

Figure 5.1: Simulated and Measured $C\left(4,2\right)$ Nodal Insertion and Return Loss, Planar Geometry, 300KHz to 1.3GHz.

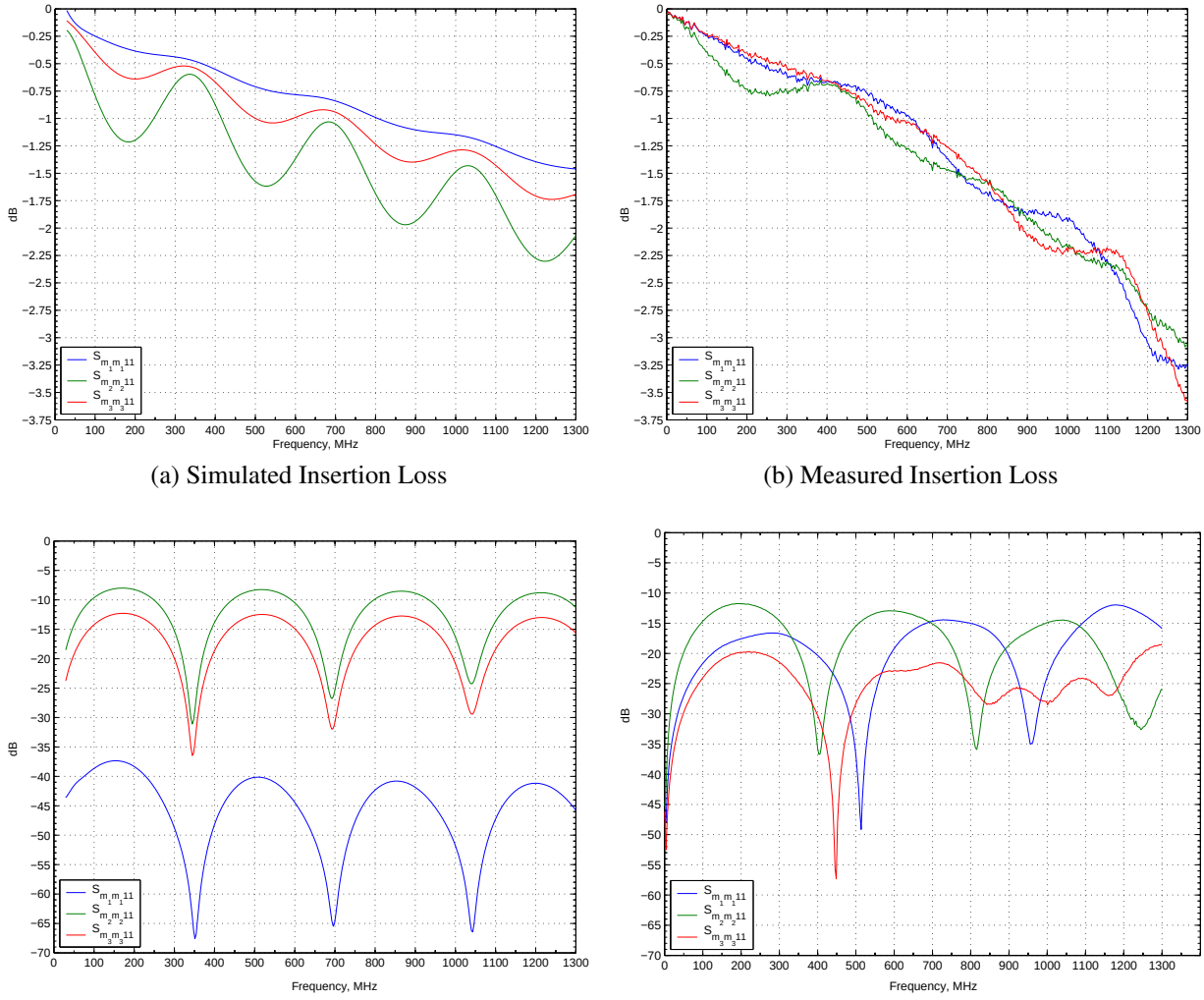

(a) Simulated Insertion Loss

(b) Measured Insertion Loss

(c) Simulated Return Loss

(d) Measured Return Loss

Figure 5.2: Simulated and Measured $C\,(4,2)$ Multi-Modal Insertion and Return Loss, Planar Geometry, 300KHz to 1.3GHz.

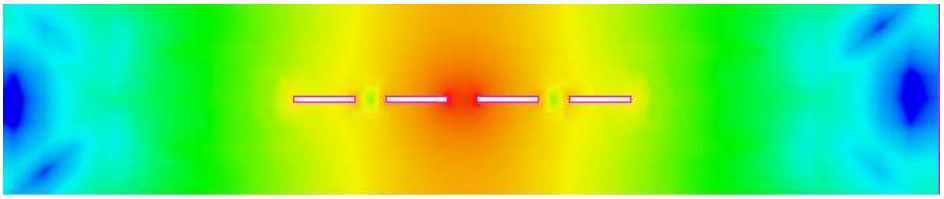

(a) Codeword {1,1,-1,-1}

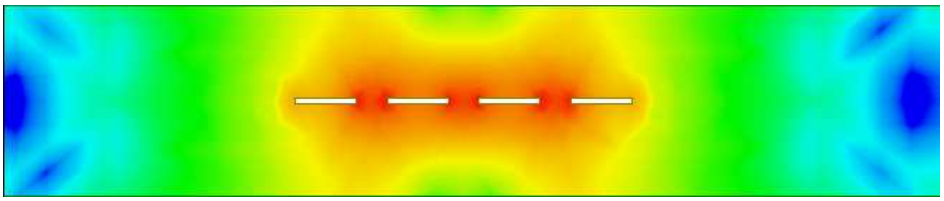

(b) Codeword {1,-1,1,-1}

Figure 5.3: Electrostatic Field Plots of Two MBDS Codewords with a 100mV Relative Differential Voltage Difference.

The asymmetry has a noticeable impact on the modal return loss S_{m_1}. This indicates that the solution modes that are propagating inside the transmission line structure for m_1 have a characteristic impedance that is much closer to the modal impedance than any of the other modes leading to lower loss.

The $C\,(4,2)$ link also gives insight to the behavior of coupled differential signals in addition to MBDS signals. Each MBDS link analysis with even m and n equal to $\lfloor \frac{m}{2} \rfloor$ captures the behavior of the subset of $\frac{m}{2}$ parallel differential links. This behavior in a $C\,(4,2)$ captured by S_{m_2} and S_{m_3} behavior in Figures 5.1 and 5.2. It can be seen that on average MBDS codewords have similar losses to two coupled differential channels and in certain cases outperforms such channels with lower modal power loss for valid MBDS modes that would not exists on parallel differential channels.

5.1.2 Square Geometry

The results of the simulations and measured response of the $C\,(4,2)$ MBDS link from 300KHz to 1.3GHz for the square geometry are shown in Figures 5.4 and 5.5. The plots contain the insertion loss and the return loss of both the nodal and multi-modal s-parameters.

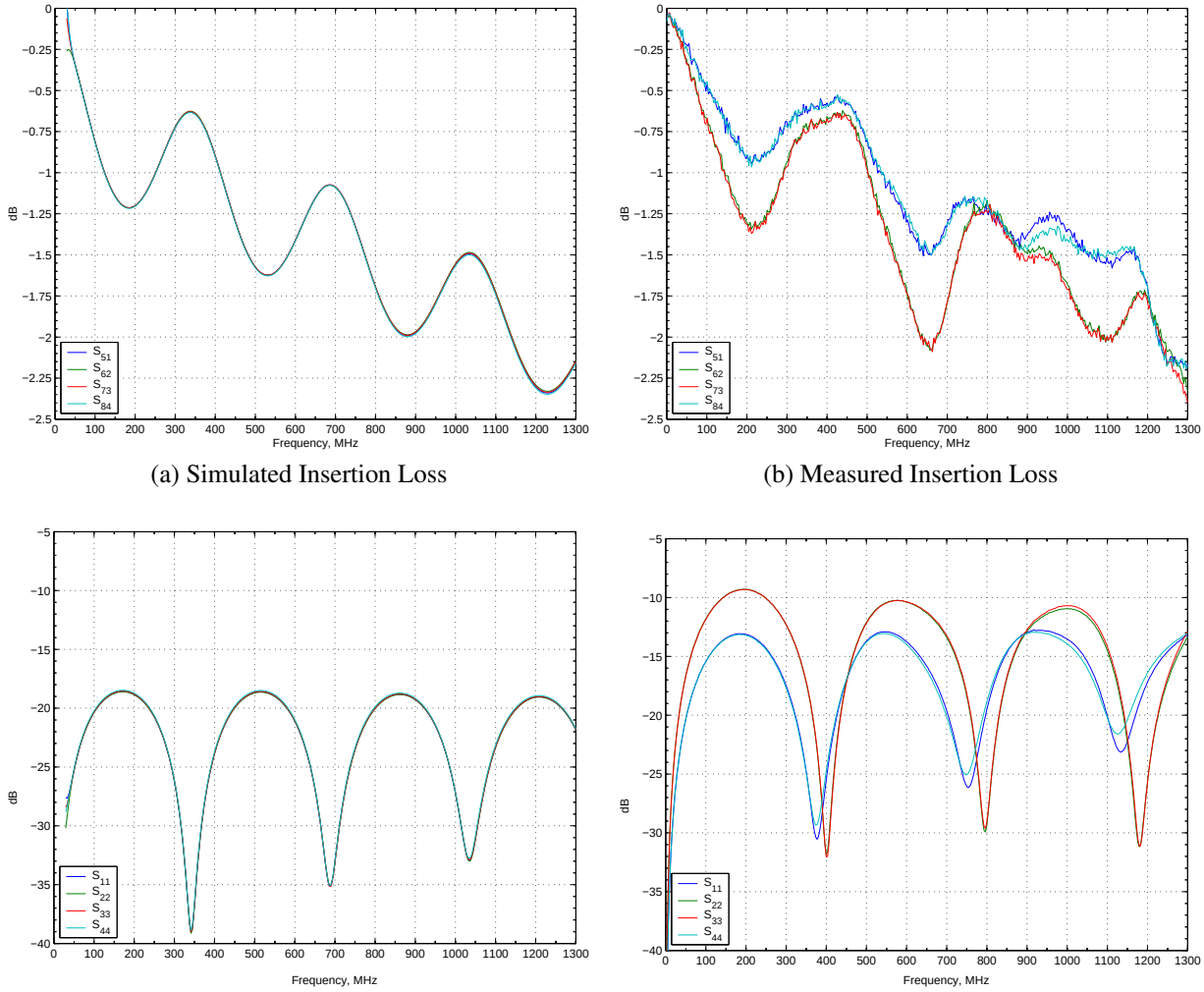

(a) Simulated Insertion Loss

(b) Measured Insertion Loss

(c) Simulated Return Loss

(d) Measured Return Loss

Figure 5.4: Simulated and Measured $C\,(4,2)$ Nodal Insertion and Return Loss, Square Geometry, 300KHz to 1.3GHz.

The square layout has the property that both the simulated insertion loss and the return loss are identical for all traces in the nodal space. The high degree of symmetry in both the horizontal and

vertical directions allow each trace to effectively see the same coupling as any of it's neighbors. However, unlike the planar geometry, the square geometry has a higher return loss of some modes over the frequency range leading to a higher overall loss in the insertion loss.

The measured data presented in Figures 5.4b and 5.4d do not behave in such a tight fashion. Referring to Figure 4.1, traces one and four are equal throughout the frequency range and are both fabricated on the same layer of the PCB. Traces two and three exhibit the same effect and are also co-planar. The manufacture of the PCB claimed different layer thickness tolerances for the two places that these traces are patterned on suggesting that the copper thickness of these signal layers is different.

$S_{m_1 m_1 21}$ displays a 20dB lower return loss and as a result shows has a lower insertion loss than the other modes for the square structure. Figure 5.5 indicates that there can be a strong dependence on the particular codeword being transmitted and the channel behavior. Mode one in the square geometry in both the simulated and measured data has lower insertion and return loss than modes two or three indicating this codeword couples very well into the PCB. Mode one is a preferred mode while mode two has the highest return loss and the lowest power output at the terminus of the PCB and should be avoided if possible in the construction of the MBDS link with this geometry.

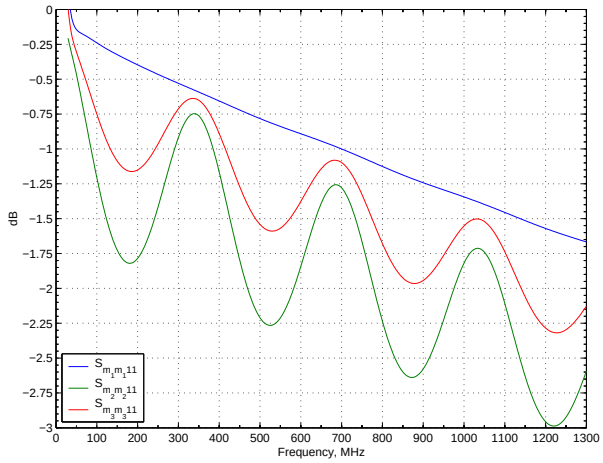

(a) Simulated Insertion Loss

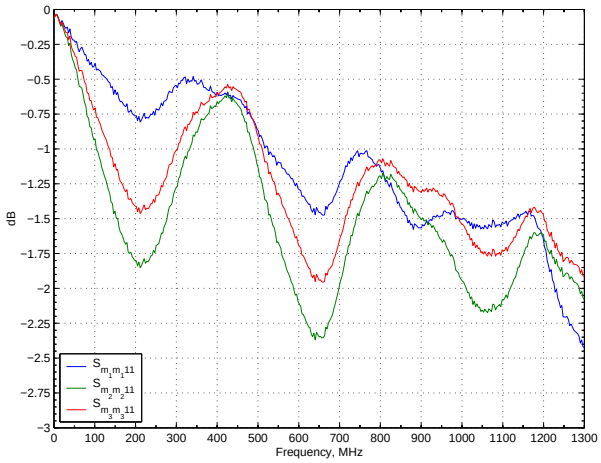

(b) Measured Insertion Loss

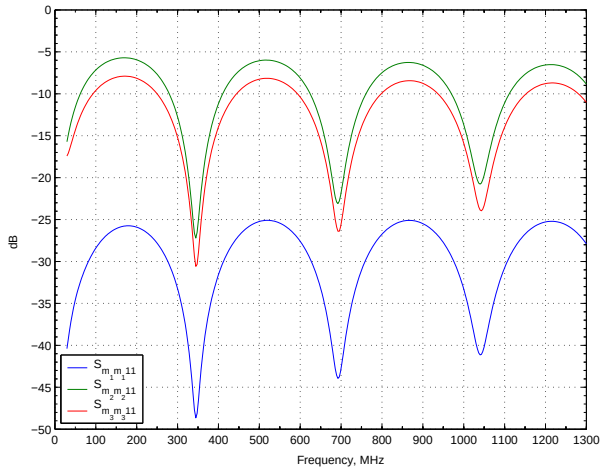

(c) Simulated Return Loss

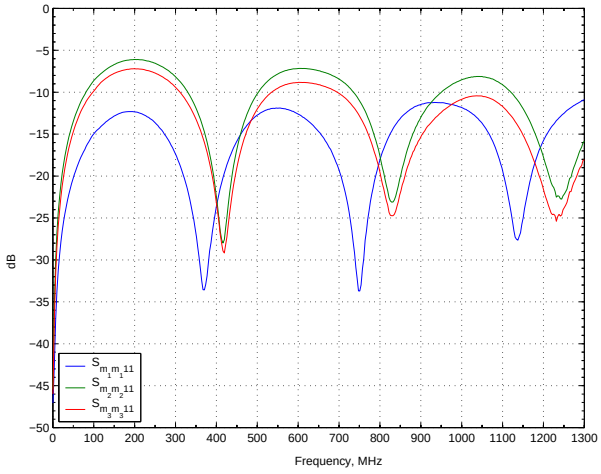

(d) Measured Return Loss

Figure 5.5: Simulated and Measured $C(4,2)$ Multi-Modal Insertion and Return Loss, Square Geometry, 300KHz to 1.3GHz.

5.1.3 Star Geometry

The results for the eight inch simulations and measured results for the $C\,(4,2)$ for the star geometry from 300KHz to 1.3GHz are shown in Figures 5.6 and 5.7. The plots show the insertion loss and the return loss in both the nodal and multi-modal space.

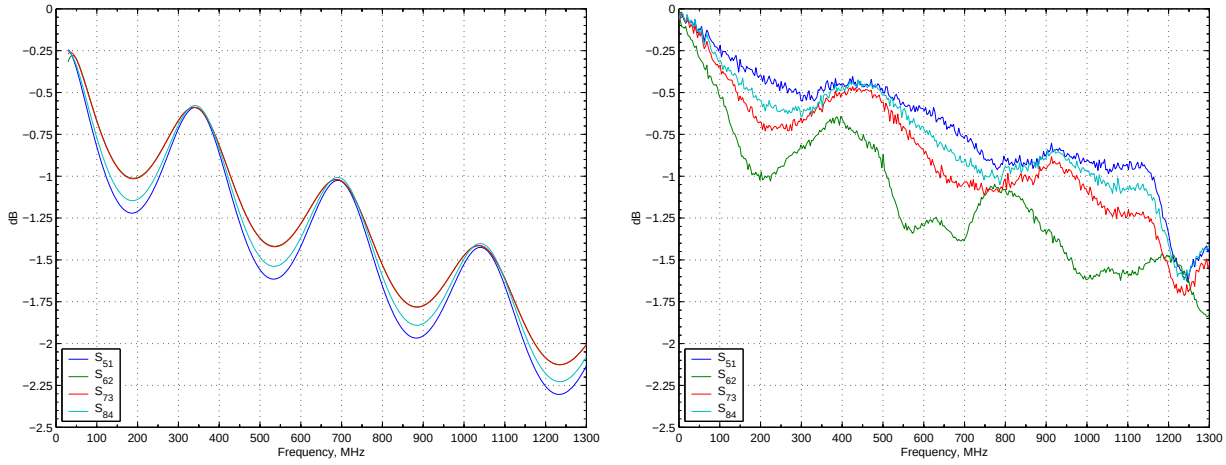

(a) Simulated Insertion Loss

(b) Measured Insertion Loss

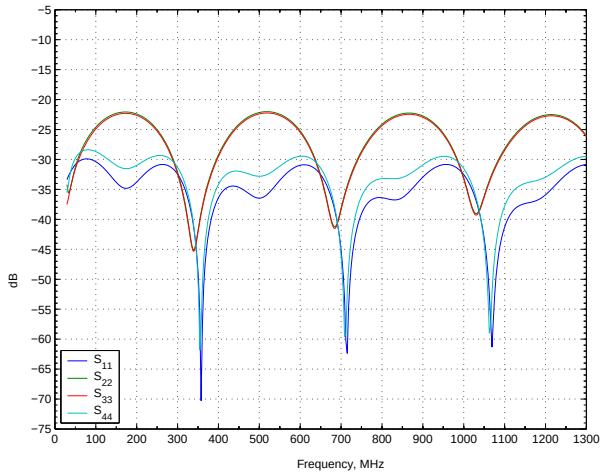

(c) Simulated Return Loss

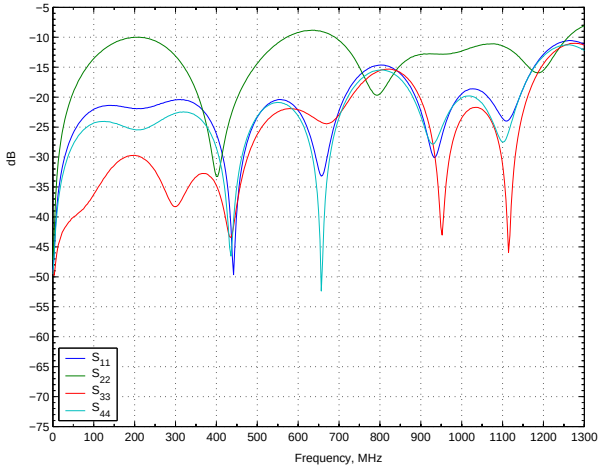

(d) Measured Return Loss

Figure 5.6: Simulated and Measured$C\,(4,2)$ Nodal Insertion and Return Loss, Star Geometry, 300KHz to 1.3GHz.

The return loss in the nodal indicates that the characteristic impedance of the conductors are not equal. *Designer* reports that at 2.5GHz the characteristic impedance of traces two and three are

42Ω with the remaining traces at 52Ω. *Designer* calculates the s-parameters using ideal 50Ω ports that couple the power waves into the star geometry with lower return loss than the reference plane of the network analyzer causing the shift between Figures 5.6c and 5.6d.

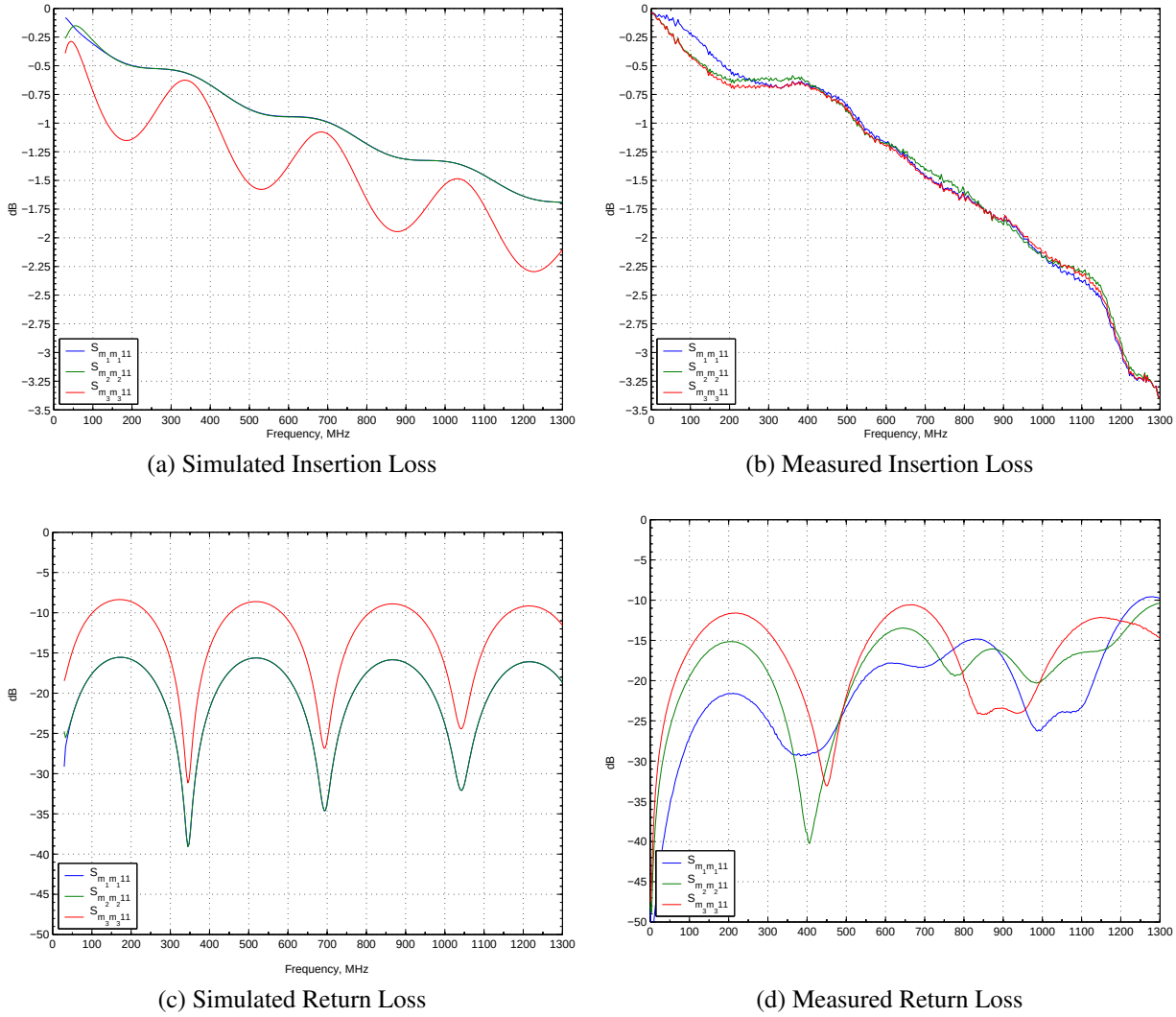

(a) Simulated Insertion Loss

(b) Measured Insertion Loss

(c) Simulated Return Loss

(d) Measured Return Loss

Figure 5.7: Simulated and Measured $C\,(4,2)$ Multi-Modal Insertion and Return Loss, Star Geometry, 300KHz to 1.3GHz.

The differences between the trace impedances causes the simulated multi-modal response to fracture depending on the driven mode introduced to the structure as can be seen in Figure 5.7b. However, the differences between the ideal simulated multi-modal ports and the real measurement ports cause the measured multi-modal response to behave in an equal manner as shown in Figure

5.7c. The unequal characteristic impedance of this structure should be avoided as the results become more dependent on the actual ports used to measure the S-parameters and higher return loss associated with port impedance mismatches.

5.1.4 High Frequency Simulations

High frequency operation of structures presented in this thesis is also simulated in the range from 500MHz to 25GHz with the representative modal responses of of the various geometries are presented in Figure 5.8. Differential and common modes of propagation are shown in these plots.

Insertion loss for all the structures decays rapidly in the high frequency range. Approaching 25GHz, both the planar and the star geometry have some modes with lower forward term loss than the square geometry with the relative differences negligible compared to the absolute loss of each mode. Return loss at high frequencies provides the best differentiation for these the structures. All layouts have very low return loss for S_{m_1} with the star and planar geometries having a lower S_{m_3} return loss than the square structure. If the excess codeword capability of the MBDS link is not required then all codewords corresponding to this mode should be discarded to allow for the highest coupling into the transmission line.

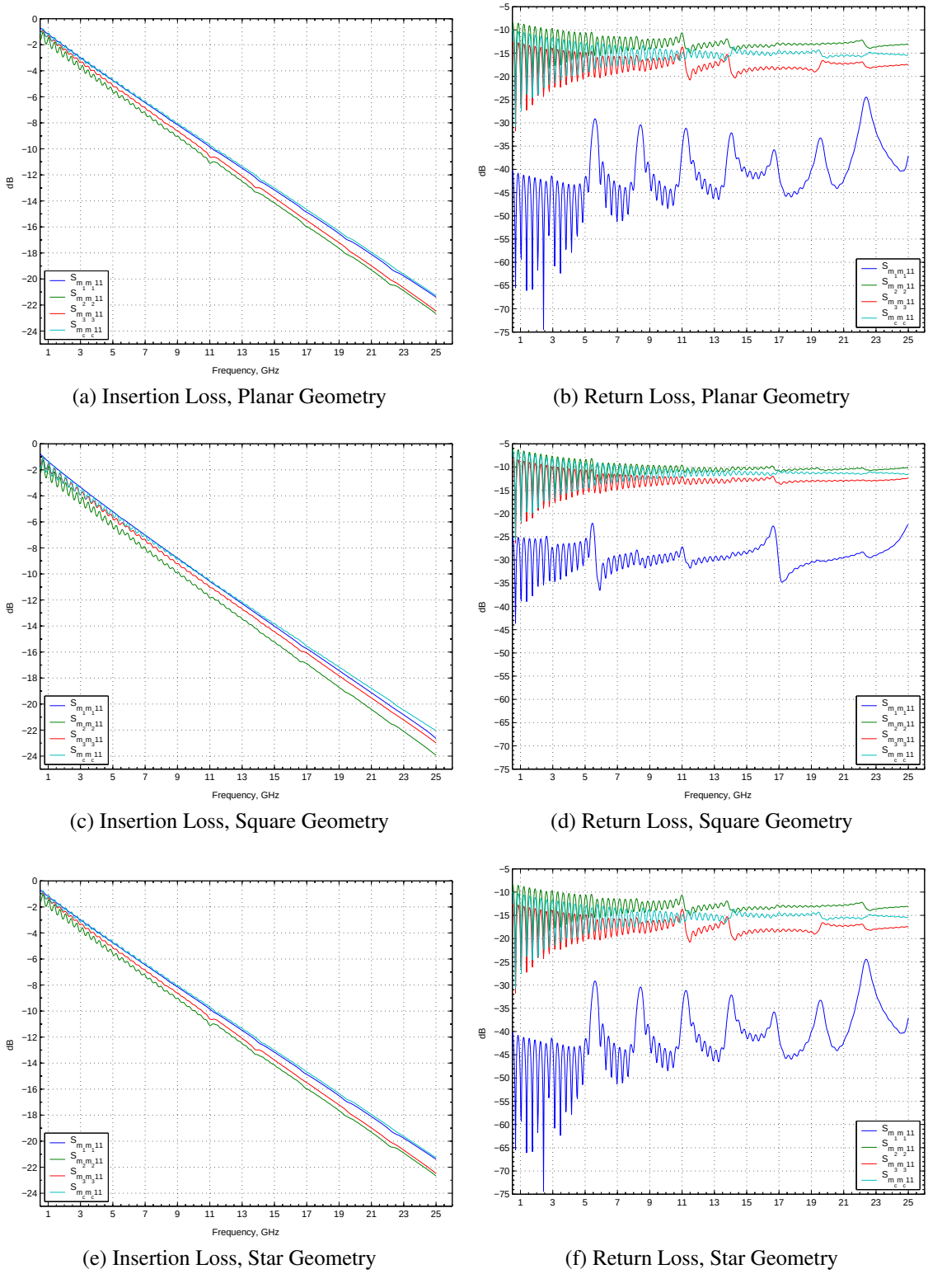

(a) Insertion Loss, Planar Geometry

(b) Return Loss, Planar Geometry

(c) Insertion Loss, Square Geometry

(d) Return Loss, Square Geometry

(e) Insertion Loss, Star Geometry

(f) Return Loss, Star Geometry

Figure 5.8: Simulated and Measured $C\,(4,2)$ Multi-Modal Insertion and Return Loss for Planar, Square and Star Geometries, 500MHz-25GHz.

5.2 SIX CHOOSE THREE RESULTS

The multi-modal simulation and measured results for the $C\,(6,3)$ links with the geometries listed in Figure 4.1 are presented here for all twenty differential modes. The common mode of propagation is not shown in these figures. Compared to the $C\,(4,2)$, for all the links presented here, there is more variation among the different insertion loss S-parameters as it becomes increasingly harder to create a symmetric structures in the high aspect ratio environment of printed circuit boards. The return loss of these simulated geometries display how strongly certain modes can naturally couple into the structure than other modes.

5.2.1 Planar Geometry

The multi-modal behavior of the planar geometry is shown in Figure 5.9. The simulated and measured multi-modal S-parameters do not entirely agree for the planar geometry and are related to the phases of the individual nodal S-parameter signals. Stimulating physical port one with codeword $\{1,1,1,-1,-1,-1\}$, as an example, a phase shift of any of individual nodes causes a fraction of the modal power to be transferred into other modes. This can be seen by the differences between the simulated return loss, Figure 5.9c, and the measured return loss shown in Figure 5.9d. Phase shift differences in the individual nodal responses cause the peaks and valleys of the return loss in the modal space to add to a more complicated response than the ideal simulated reference port. The sources of these phase shifts include the longer trace lengths necessary to break out the transmission line structure into the SMA's connecting the network analyzer to the PCB while avoiding vias. The nodal insertion loss S-parameters are shown in Figure 5.10 for comparison.

5.2.2 Square Geometry

The magnitude of the multi-modal insertion loss of the measured and simulated responses shown in Figure 5.11 show less differences than the planar structure presented in Section 5.2.1. Comparing the simulated and measured return loss plots for this structure again show that the phases of the measured nodal responses are impacting the behavior of the multi-modal response.

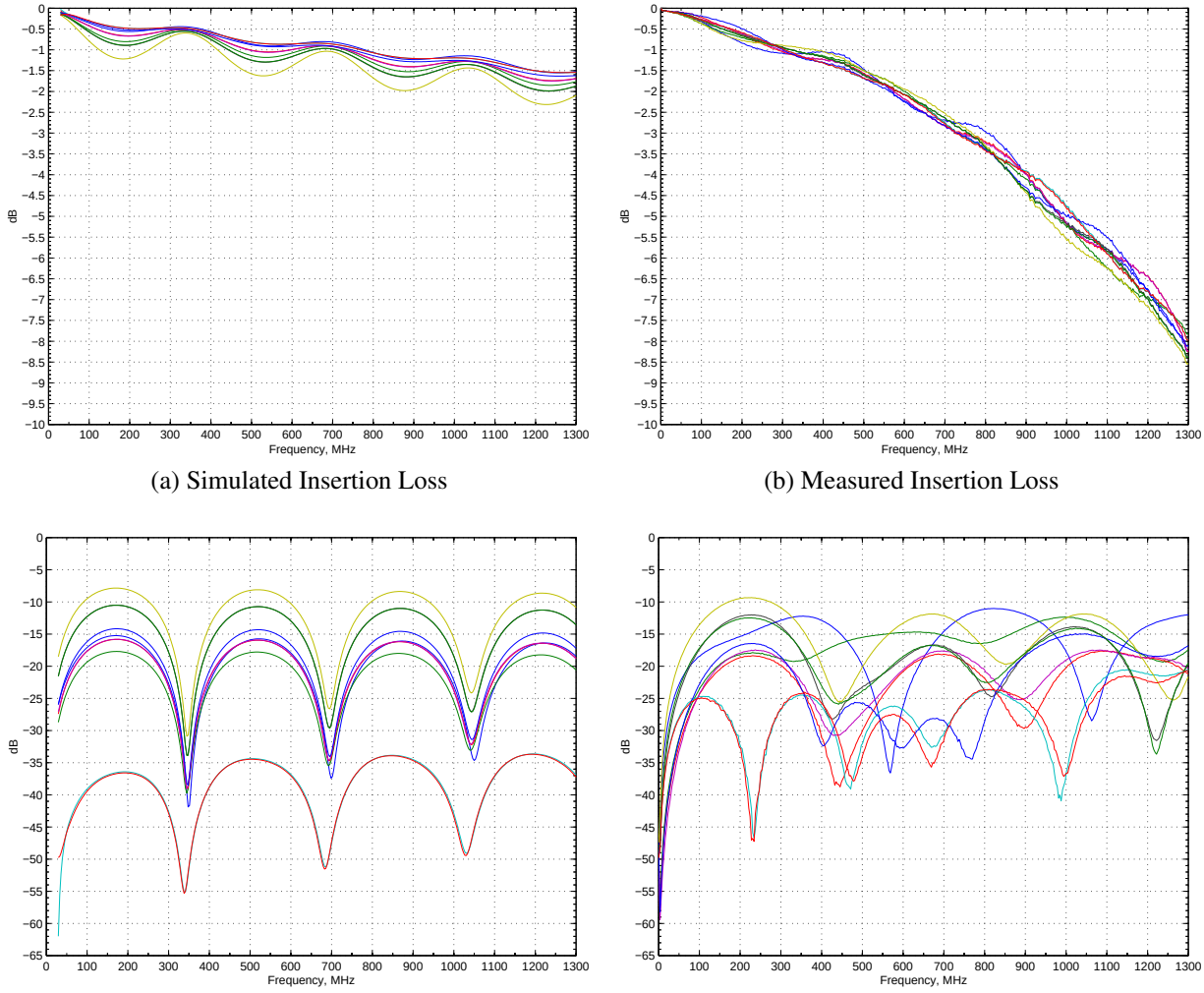

(a) Simulated Insertion Loss

(b) Measured Insertion Loss

(c) Simulated Return Loss

(d) Measured Return Loss

Figure 5.9: Simulated and Measured $C\,(6,3)$ Multi-Modal Insertion and Return Loss, Planar Geometry, 300KHz to 1.3GHz.

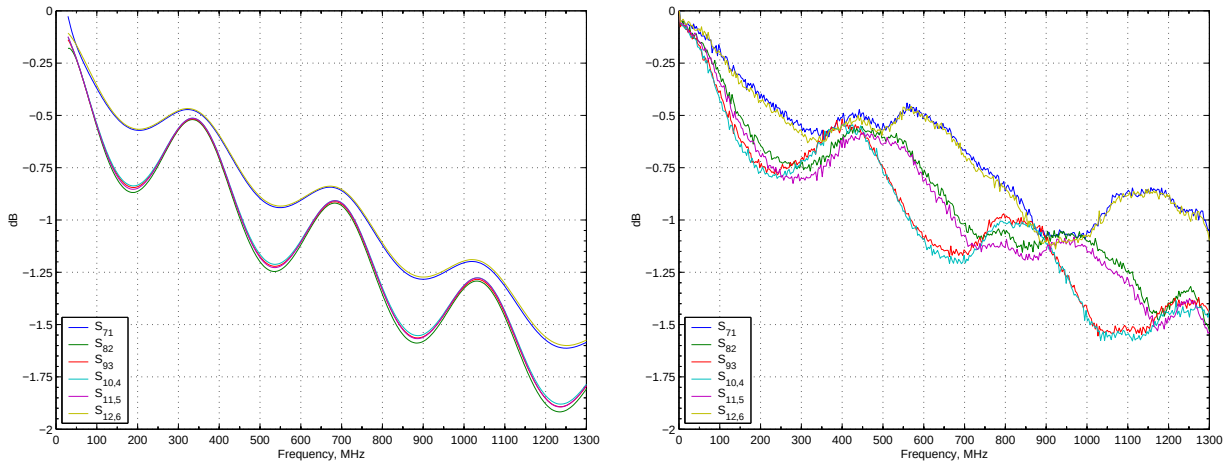

(a) Simulated Insertion Loss

(b) Measured Insertion Loss

Figure 5.10: Simulated and Measured $C\,(6,3)$ Nodal Insertion and Return Loss, Planar Geometry, 300KHz to 1.3GHz.

5.2.3 Star Geometry

The multi-modal simulated and measured S-parameters of the $C\,(6,3)$ star structure are shown in Figure 5.12. Similar to the square and planar geometries the return loss differences between the simulated and measured structure display the impact of the non-ideal ports used to measure the structure. Even with these differences, the measured insertion losses and return losses of the differential modes are less than simulation predicts indicating that the characteristic modal impedance of the PCB matches the reference plane better than the ideal simulated ports. The differences between the simulations and the measured data can also be attributed to the differing characteristic impedance of traces one and six of the star structure as reported by *Designer*, similar to the effects of the $C\,(4,2)$ star structure.

Comparing the measured insertion loss of Figures 5.9b, 5.11b and 5.12b the star and square structures have lower loss that the planar structure. Due to the differing characteristic impedances of the traces of the star structure and the co-equal modal behavior of the square structure indicates that the square structure presented in this thesis is a good candidate for implemented $C\,(6,3)$ links.

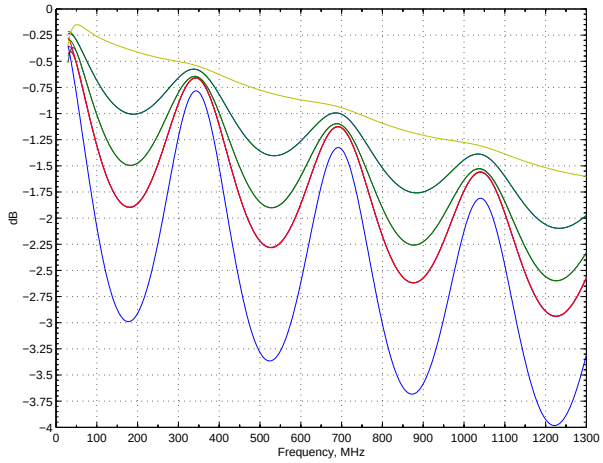

(a) Simulated Insertion Loss

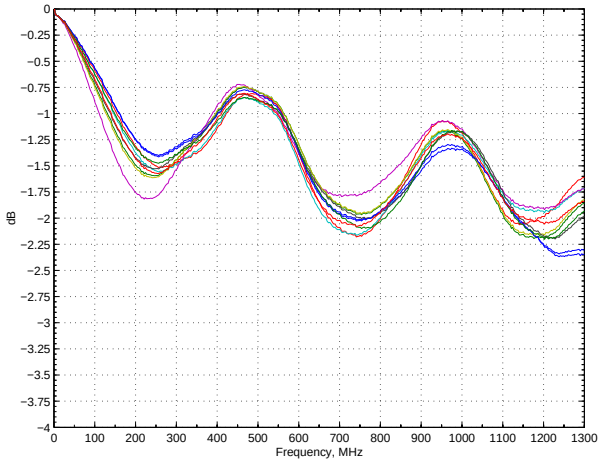

(b) Measured Insertion Loss

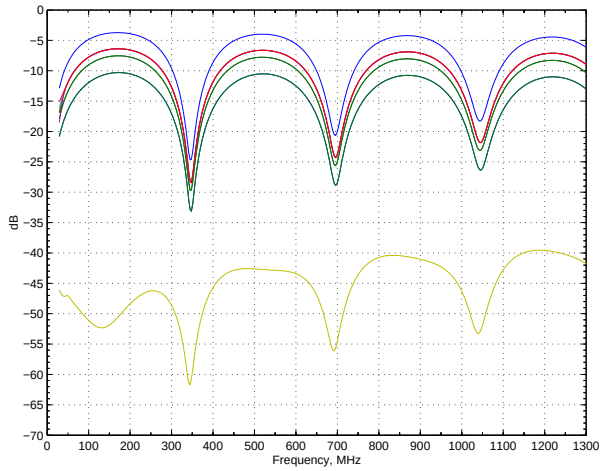

(c) Simulated Return Loss

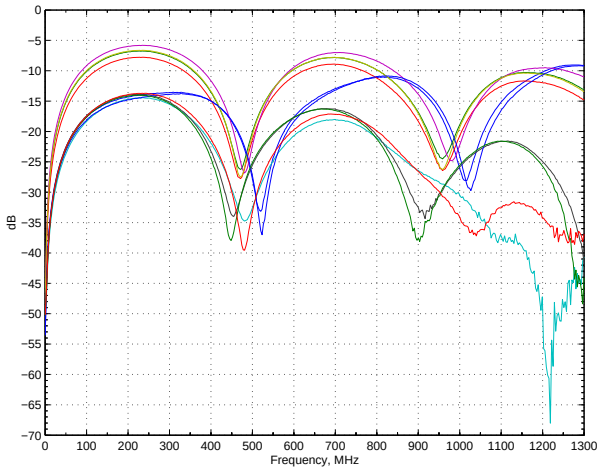

(d) Measured Return Loss

Figure 5.11: Simulated and Measured $C\,(6,3)$ Multi-Modal Insertion and Return Loss, Square Geometry, 300KHz to 1.3GHz.

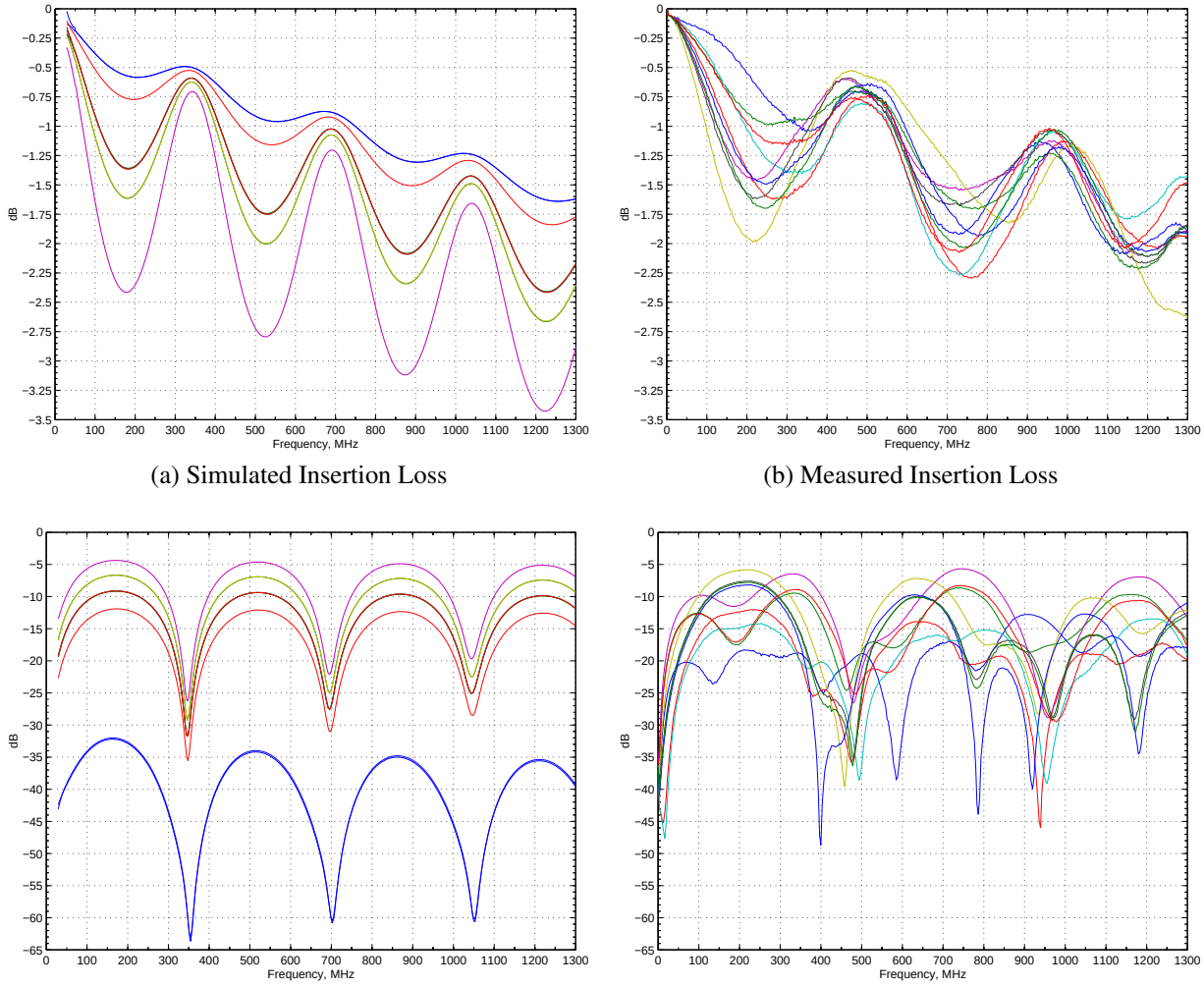

(a) Simulated Insertion Loss

(b) Measured Insertion Loss

(c) Simulated Return Loss

(d) Measured Return Loss

Figure 5.12: Simulated and Measured $C\,(6,3)$ Multi-Modal Insertion and Return Loss, Star Geometry, 300KHz to 1.3GHz.

5.2.4 High Frequency Simulations

The high frequency simulations show the same high-loss behavior in the PCB as in the four choose two case. These results are displayed in Figure 5.13. At frequencies above 5GHz, the relative differences in modal propagation become constants functions. Above 5GHz the relative loss of the modes to each other is becoming much less significant than the total loss of each mode. Decreasing amount of power loss in the PCB at these frequencies is material dependent than structure dependent.

5.3 MODIFIED SIX CHOOSE THREE STAR GEOMETRY

The star geometry was modified through a trial an error approach using *Ansoft HFSS* to bing the impedance of each conductor closer to matching the reference impedance of 50Ω as the reference plane. The modified star geometry is listed in Figure 5.14.

The multi-modal insertion and return loss for this structure are shown in Figure 5.15. Even with the optimization of the impedance matching, the star structure retains the high return loss shown in Figures 5.12a and 5.12b. Some of the modal insertion loss terms do show less loss but compared to the original geometry the modified star geometry does not show significant improvement.

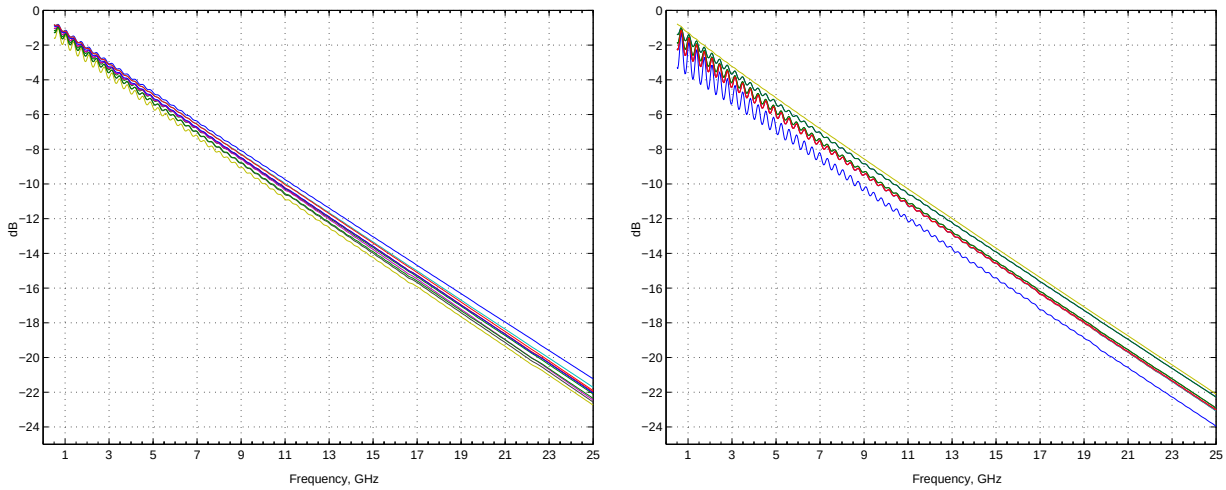

(a) Planar Geometry

(b) Square Geometry

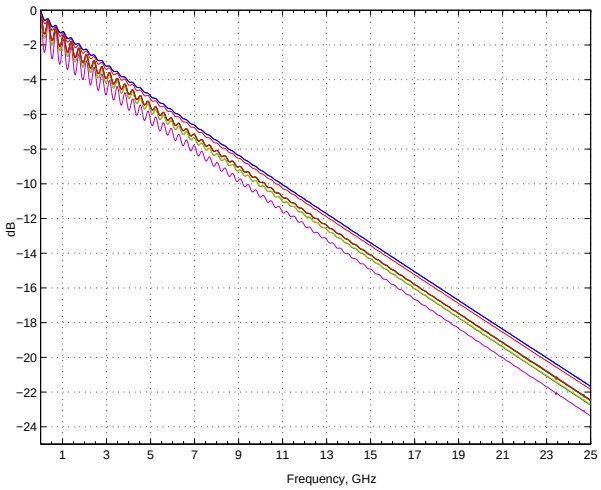

(c) Star Geometry

Figure 5.13: Simulated $C\left(6,3\right)$ Multi-Modal Insertion Loss for the Planar, Square and Star Geometries, 500MHz-25GHz.

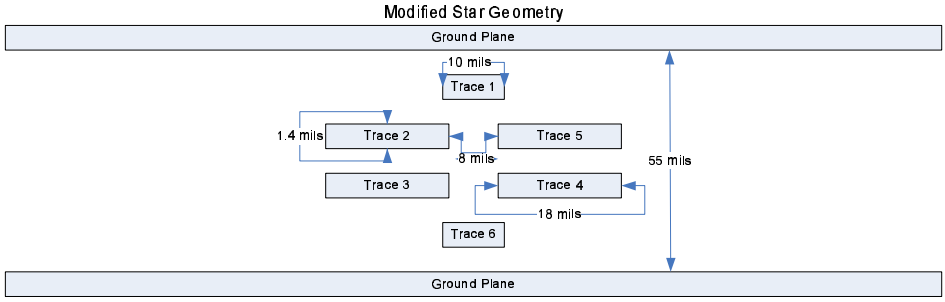

Figure 5.14: Modified $C\,(6,3)$ Star Geometry.

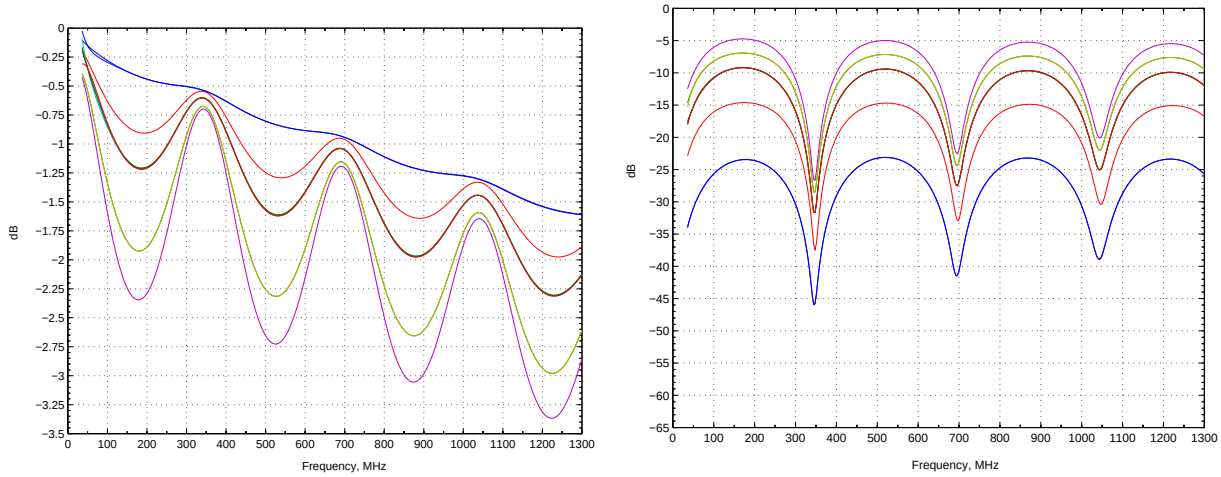

(a) Insertion Loss, Modified Star Geometry

(b) Return Loss, Modified Star Geometry

Figure 5.15: Simulated $C\,(6,3)$ Multi-Modal S-Parameters, Modified Star Geometry, 300kHz-1.3GHz.

6.0 CONCLUSIONS

6.1 CONTRIBUTIONS OF THE ANALYSIS

This work demonstrates a method where a multi-bit differential signaling channel is characterized. The method presented allows for the analysis of any MBDS channel configuration. The formulation also provides a method where parallel differential channels that are close in proximity can be analyzed to determine the effects each channel will have on the other.

It is also shown that the channel configuration can impact the loss of power delivered to and the power transmitted by the channel and that this loss can be dependent on the particular MBDS codeword being transmitted across the channel. Configurations where there is a loss of symmetry of each conductor relative to it's neighbors will cause the modal loss in the system to be codeword dependent. This loss can be overcome by changing either the geometry of the channel or using the excess codewords in the code-set to remove those codewords with high loss. For the $C\left(4,2\right)$ and $C\left(6,3\right)$ MBDS links the square geometry has the lowest overall loss or has the most similar multi-modal characteristics of the configurations shown in Figure 4.1 and Figure 4.2.

Of the structures presented in this paper, the greatest impact on the MBDS multi-modal space occurs due to changes in the direction perpendicular to the plane of the PCB. The jump from $C\left(4,2\right)$ to $C\left(6,3\right)$ causes a greater variation in the modal responses of the square and star structure than was observed in the $C\left(4,2\right)$ case due to the extra PCB layer. Conversely, modifying the star geometry to bring the impedances of each trace equal to each other does not improve the overall multi-modal response of the structure.

6.2 FUTURE RESEARCH

Further work can be conducted into the ability to properly terminate the transmission line structure and provide the proper common node voltage reference in the MBDS channel. The complex geometries presented in this paper and any other feasible layout may not be optimally terminated with the star termination network MBDS utilizes to generate the common node voltage. A termination network that properly matches the transmission line structure may not generate the proper voltage levels necessary for MBDS. Using the multi-modal S-parameters it may be possible to build a hybrid termination structure that provides proper transmission line termination and MBDS voltage levels.

Characterization of the channels presented in this thesis is performed by calculating $\mathbf{S}_{mm}$ after measuring $\mathbf{S}_n$. Using the techniques presented in this thesis a conceptual pure-mode network analyzer could be constructed where the network is stimulated with MBDS codewords and the measured response used to calculate multi-modal S-parameters.

BIBLIOGRAPHY

[1] J. D. Bakos, *Lightweight Hierarchical Error Control Codes for Multi-Bit Differential Channels*. Ph.D. dissertation, University of Pittsburgh, 2005.

[2] D. Bockelman, *The Theory, Measurement, and Applications of Mode Specific Scattering Parameters with Multiple Modes of Propagation*. Ph.D. dissertation, University of Florida, 1997.

[3] D. Bockelman and W. Einstadt, "Pure-mode network analyzer for on-wafer measurements of mixed-mode s-parameters of differential circuits," *IEEE Transactions on Microwave Theory and Techniques*, vol. 45, pp. 1071–1077, July 1997.

[4] D. Bocklman and W. Einstadt, "Combined differential common-mode scattering parameters: Theory and simulation," *IEEE Transactions on Microwave Theory and Techniques*, vol. 43, pp. 1530–1539, July 1995.

[5] D. Chiarulli, J. Bakos, J. Martin, and S. Levitan, "Area, power, and pin efficient bus transceiver using multi-bit-differential signaling," in *IEEE International Symposium on Circuits and Systems*, vol. 2, pp. 1662–1665, ISCAS, IEEE, May 2005.

[6] S. Cohn, "Shielded coupled-strip transmission lines," *IRE Transactions on Microwave Theory and Technology*, vol. MTT-3, pp. 8–12, 1955.

[7] W. Fan, A. Lu, L. Wai, and B. Lok, "Mixed-mode s-parameter characterization of differential structures," in *Electronics Packaging Technology, 2003 5th Conference*, pp. 533–537, EPTC 2003, IEEE, Dec 2003.

[8] J. Faria, *Multi-conductor Transmission-Line structures: Modal Analysis Techniques*. Wiley Series in Microwave and Optical Engineering, New York, New York: John While & Sons, Inc., 1993.

[9] C. Ferland, "Just what is LVDS?," *IEE Electronic Systems and Software*, vol. 2, pp. 36–37, December-January 2004-2005.

[10] HyperTransport Technology Consortium, http://www.hypertransport.org/docs/tech/HTC20051222-0046-0008-Final-4-21-06.pdf, *HyperTransport I/O Link Specification, Revision 3.00*, 2006.

[11] K. Kurokawa, "Power waves and the scattering matrix," *IEEE Transactions on Microwave Theory and Techniques*, vol. MTT-13, pp. 194–202, March 1965.

[12] R. Ludwig and P. Bretchko, *RF Circuit Design: Theory and Applications*. Upper Saddle River, New Jersey: Prentice Hall, Inc., 2000.

[13] K. Marx, "Propagation modes, equivalent circuits, and characteristic terminations for multiconductor transmission lines with inhomogeneous dielectrics," *IEEE Transactions on Microwave Theory and Techniques*, vol. MTT-21, pp. 450–457, July 1973.

[14] D. Miller and H. Ozaktas, "Limit to the bit-rate capacity of electrical interconnects from the aspect ratio of the system architecture," *Journal of Parallel and Distributed Computing*, vol. 41, pp. 42–52, Feb 1997.

[15] R. Newcomb, *Linear Mulitport Synthesis*. McGraw-Hill Electronic Sciences Series, McGraw-Hill Book Company, 1966.

[16] V. Tripathi, "Asymmetric coupled transmission lines in an inhomogeneous medium," *IEEE Transactions in Microwave Theory and Techniques*, vol. MTT-23, pp. 734–739, September 1975.